# EAVN Status Report for the 2022A Semester

EAVN User Support Team, KASI, NAOJ, SHAO, XAO, YNAO, NGII, Ibaraki University, and Yamaguchi University

September 24, 2021

## Additional notification to EAVN proposers (revised on 2021 October 8 and 14)

- An additional condition on the usage of Yamaguchi station (YAM32) was added to the status report. Please refer to Section 3.1.1 (p.34) for more details. (Revised on 2021 October 8)
- A detailed condition on time allocation of Nobeyama station (NRO45) was changed. Please refer to Section 3.1.2 (p.35) for more details. (Revised on 2021 October 14)

## Major revision since the 2022A semester

- New telescope "Sejong" (KSJ) at K and Q-band (Section 2.2.11 and related figures/tables)
- Possible time slots in LST for NRO45 (Section 3.1.2)
- Instruction of schedule preparation using NRAO sched (Section 5.1.1)
- Instruction of data reduction recipes (Section 5.3.1)

## Contents

1	Intr	oducti	on	5											
2	Sys	System													
	2.1	Array		5											
	nas	9													
		2.2.1	Brief Summary of VERA Antennas	9											
		2.2.2	Brief Summary of KVN Antennas	10											
		2.2.3	Nobeyama 45-m Telescope	10											
		2.2.4	Takahagi 32-m Telescope	10											
		2.2.5	Hitachi 32-m Telescope	11											
		2.2.6	Yamaguchi 32-m Telescope	11											
		2.2.7	Tianma 65-m Telescope	11											
		2.2.8	Sheshan 25-m Telescope	12											
		2.2.9	Nanshan 26-m Telescope	12											
		2.2.10	Kunming 40-m Telescope	12											
		2.2.11	Sejong 22-m Telescope	12											
		2.2.12	Aperture Efficiency	13											
		2.2.13	Beam Pattern and Size	15											
	2.3	Receiv	ers	16											
		2.3.1	Brief Summary of VERA Receiving System	16											
		2.3.2	Brief Summary of KVN Receiving System	17											
		2.3.3	Brief Summary of NRO45 Receiving System	19											
		2.3.4	Brief Summary of TAK32 Receiving System	19											
		2.3.5	Brief Summary of HIT32 Receiving System	21											
		2.3.6	Brief Summary of YAM32 Receiving System	21											
		2.3.7	Brief Summary of TMRT65 Receiving System	22											
		2.3.8	Brief Summary of SHRT25 Receiving System	23											
		2.3.9	Brief Summary of NSRT26 Receiving System	23											
		2.3.10	Brief Summary of KMRT40 Receiving System	24											
		2.3.11	Brief Summary of KSJ Receiving System	24											
	2.4	Digital	l Signal Processing	24											
	2.5		lers	25											
		2.5.1	Note on the Data Storage Capacity	25											
	2.6	Correla		28											
	ū	2.6.1	Note for the C2 Mode	28											
	2.7	Calibra		29											
	•	2.7.1	Delay and Bandpass Calibration	29											

		2.7.2	Gain Calibration	29						
		2.7.3	Pointing Correction	31						
	2.8	Geode	tic Measurement	31						
		2.8.1	Brief Summary of VERA Geodetic Measurement	31						
		2.8.2	Brief Summary of KVN Geodetic Measurement	32						
3	Obs	erving	Proposal	33						
	3.1	Call fo	or Proposals (CfP)	33						
		3.1.1	Total telescope time and maximum of total request time (see Table 9)	33						
		3.1.2	Term of EAVN observation	35						
		3.1.3	Possible array configuration	35						
	3.2	Propo	sal Submission	36						
	3.3	Specia	l Condition for Selecting Proposals	36						
	3.4	Policy	of Recovery Observations	36						
	3.5	Policy	of One-year-long Proposals	37						
	3.6	Obser	vation Mode	37						
	3.7	Possib	le Conflict/duplication with Large Programs	37						
	3.8	Target of Opportunity (ToO) Observations								
	3.9	Angular Resolution and Largest Detectable Angular Scale 3								
	3.10	0 Sensitivity								
	3.11	Calibr	ator Information	42						
	3.12	Data A	Archive	42						
4	Not	es for	Special Modes	45						
	4.1	Phase-	-referencing and Astrometry	45						
		4.1.1	Fast Switching	45						
		4.1.2	Notification for Switching Cycle in C-band	45						
		4.1.3	Separation Angle between Target and Phase Reference	45						
		4.1.4	Tropospheric Calibration with GPS or JMA or Geodetic Blocks	46						
		4.1.5	Astrometric Accuracy	46						
		4.1.6	Baseline Length	47						
		4.1.7	A priori Model of the KJCC Correlator	49						
		4.1.8	Data Reduction	49						
	4.2		n Hybrid (K/Q/W) Mode	50						
	4.3		field Imaging Mode	50						
	4.4	Simult	caneous K/Q Band Mode	52						
5	Obs	ervatio	on and Data Reduction	53						
	5.1	Prepar	ration of an EAVN Observation	53						

	5.1.1 Sample Key Files for NRAO sched	53
5.2	Observation and Correlation	54
5.3	Data Reduction	54
	5.3.1 Sample AIPS Recipes	54
5.4	Policy of User Support	55
5.5	Acknowledgment	55
5.6	Further Information	55

## 1 Introduction

This document describes the current observational capabilities as of 2021 September, and available observing time of the East Asian VLBI Network (EAVN). EAVN is the international collaborative VLBI array operated by Korea Astronomy and Space Science Institute (KASI), National Astronomical Observatory of Japan (NAOJ), Shanghai Astronomical Observatory (SHAO; China), Xinjiang Astronomical Observatory (XAO; China), Yunnan Observatories (YNAO; China), and National Geographic Information Institute (NGII; Korea).

EAVN invites proposals for open-use observations to be carried out from January 16, 2022 to June 15, 2022 (2022A semester). The total observing time of 500 hours is provided for EAVN open-use operation to proposers, while the available machine time of each telescope is different between each other. Please refer to Table 9 in Section 3 for more details.

In the 2022A semester, EAVN is operated using 16 telescopes, all four telescope of VERA, Nobeyama 45-m, Takahagi 32-m, Hitachi 32-m, and Yamaguchi 32-m telescopes in Japan, 3 telescopes of KVN and Sejong 22-m in Korea, Tianma 65-m, Sheshan 25-m, Nanshan 26-m, and Kunming 40-m telescopes in China. Sejong 22-m antenna becomes a new member of EAVN from the 2022A semester for the K and Q-band observations as a shared risk mode. Figure 1 shows location of EAVN telescopes which participate in open-use observations of EAVN in the 2022A semester.

This status report summarizes general information about EAVN and the performance of each telescope/array, and how to prepare and submit proposals for EAVN. Please refer to the latest report for the overall performance of EAVN [4].

## 2 System

## 2.1 Array

In the 2022A semester, 16 radio telescopes (KVN 3 × 21 m, VERA 4 × 20 m, Nobeyama 45 m, Takahagi 32 m, Hitachi 32 m, Yamaguchi 32 m, Tianma 65 m, Sheshan 25 m, Nanshan 26 m, Kunming 40 m, and **Sejong 22 m**) are available for EAVN open use, as shown in Figure 1. **Sejong 22 m antenna participates in the EAVN observations from the 2022A semester for the K and Q-band observations as a shared risk mode.** Three observing frequencies, 6.7 (C-band), 22 (K-band) and 43 GHz (Q-band), are opened in the 2022A semester.

KaVA (KVN and VERA Array) is a core array of EAVN, which consists of 7 antenna sites in VERA-Mizusawa, VERA-Iriki, VERA-Ogasawara, VERA-Ishigakijima, KVN-Yonsei, KVN-Ulsan and KVN-Tamna with 21 baselines in 2022A. The maximum baseline length of KaVA is 2270 km between VERA-Mizusawa and VERA-Ishigakijima stations, and the minimum baseline length is 305 km between KVN-Yonsei and KVN-Ulsan stations. The maximum angular resolution expected from the baseline length of KaVA is 6.0 mas for C-band (VERA-Ogasawara – KVN-Ulsan baseline), 1.2 mas for K-band and about 0.6 mas for Q-band. The maximum angular resolution is improved to be 2.4 mas at C-band and 0.55 mas at K-band for EAVN (the longest baseline of 3874 km for VERA-Ogasawara – Kunming and 5100 km for VERA-Ogasawara –

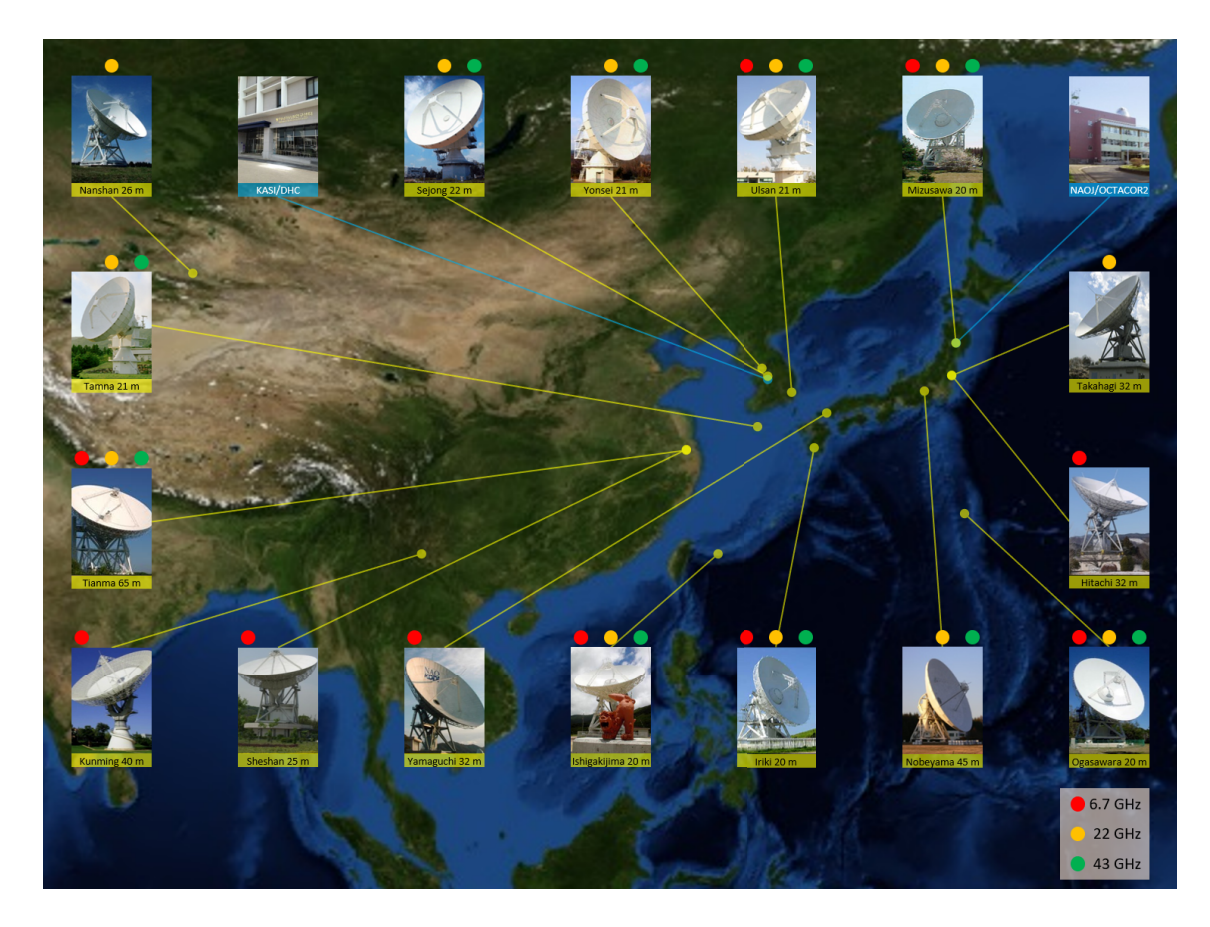


Figure 1: Location of EAVN sites, including the Korea-Japan Correlation Center at KASI (Korea) and Mizusawa VLBI observatory (NAOJ, Japan), overlaid on 'the Blue Marble' image (credit of the ground image: NASA's Earth Observatory).

Nanshan baseline, respectively), and that at Q-band was identical to that of VERA (0.63 mas for VERA-Mizusawa – VERA-Ishigakijima baseline) for the full-array of EAVN. Sejong 22-m telescope newly participates in the open-use program from the 2022A semester, resulting in making the minimum baseline length in EAVN of 120 km between Sejong and KVN-Yonsei stations. The geographic locations and coordinates of EAVN antennas in the coordinate system of epoch 2009.0 are summarized in Table 1. Figures 2 and 3 show examples of uv plane coverage for KaVA and EAVN, respectively. Figure 4 shows the elevation angle of each EAVN antenna as a function of hour angle.

The coordinates and averaged velocities of KaVA sites in Table 2 are predicted values at the epoch of January 1, 2018. Reference frame of these coordinates is ITRF2014. The rates of the coordinates of Mizusawa, Iriki, Ogasawara and Ishigakijima are the average value of change of the coordinates from April 16, 2016 to May 26, 2018, after the 2016 Kumamoto Earthquake ( $M_j = 7.3$ ). The 2011 off the Pacific coast of Tohoku Earthquake ( $M_j = 9.0$ ) brought the co-seismic large step and non-linear post-seismic movement to the coordinates of Mizusawa. Co-seismic steps of the coordinates of Mizusawa are dX = -2.0297 m, dY = -1.4111 m and dZ = -1.0758 m. The creeping continues still now, though decreased. The changes of coordinates by the post-seismic creeping are dX = -1.2148 m, dY = -0.6402 m and dZ = -0.3042 m in total from March 12, 2011 to January 1, 2020.

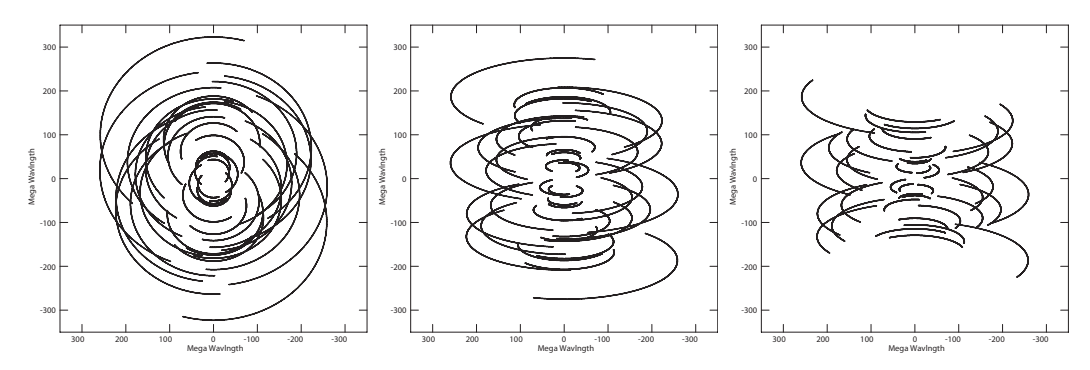


Figure 2: Examples of (u, v) coverage for an KaVA observation at Q-band with the source's declination of  $+60^{\circ}$  (left panel),  $+20^{\circ}$  (center panel), and  $-20^{\circ}$  (right panel). Total observation duration of 10 hours and the antenna's lower elevation limit of 15° are assumed for all cases.

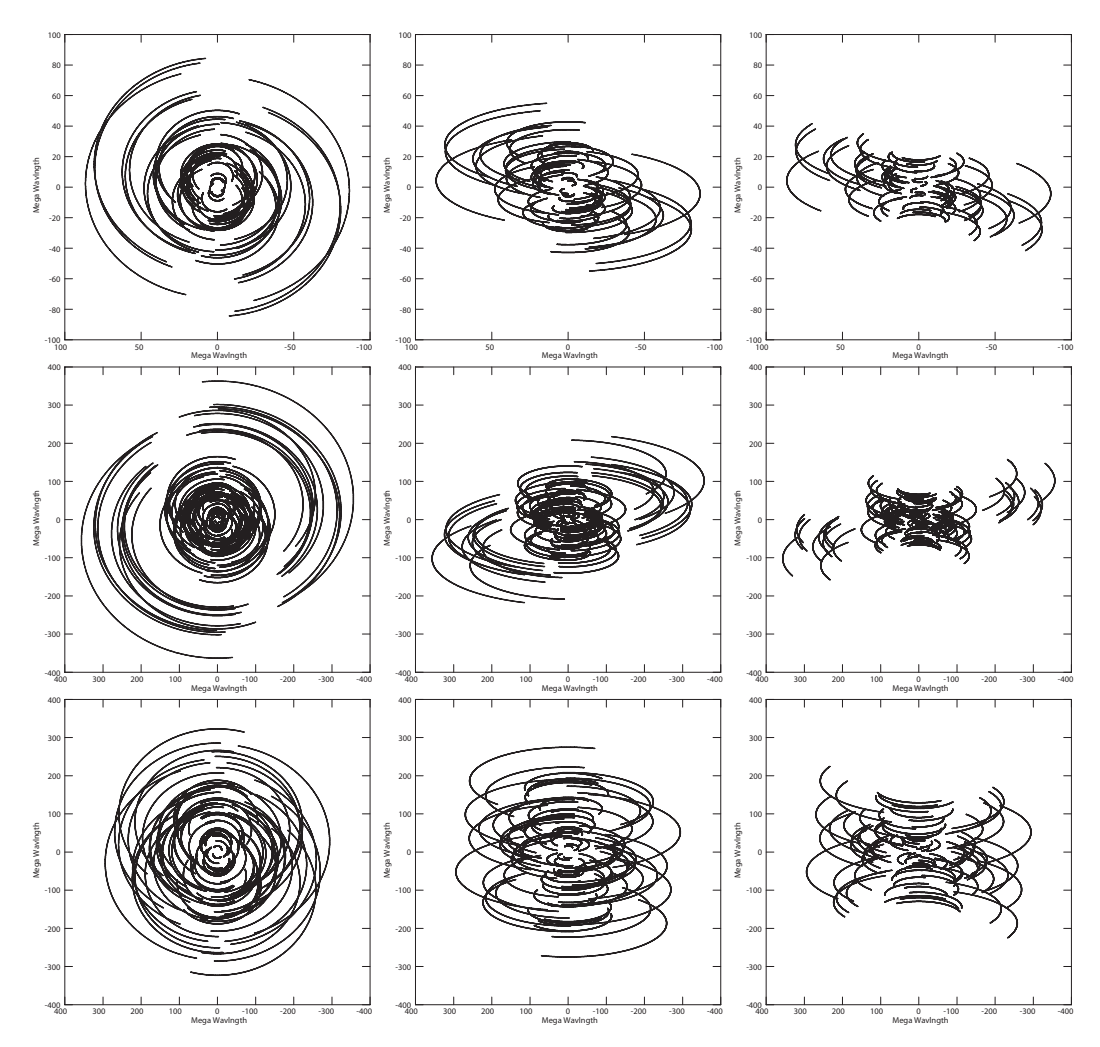


Figure 3: Examples of (u, v) coverage for an EAVN observation with full array configuration at C-band (upper panels), K-band (middle panels) and Q-band (lower panels) with the source's declination of  $+60^{\circ}$  (left panels),  $+20^{\circ}$  (center panels), and  $-20^{\circ}$  (right panels). Total observation duration of 10 hours and the antenna's lower elevation limit of  $15^{\circ}$  are assumed for all cases.

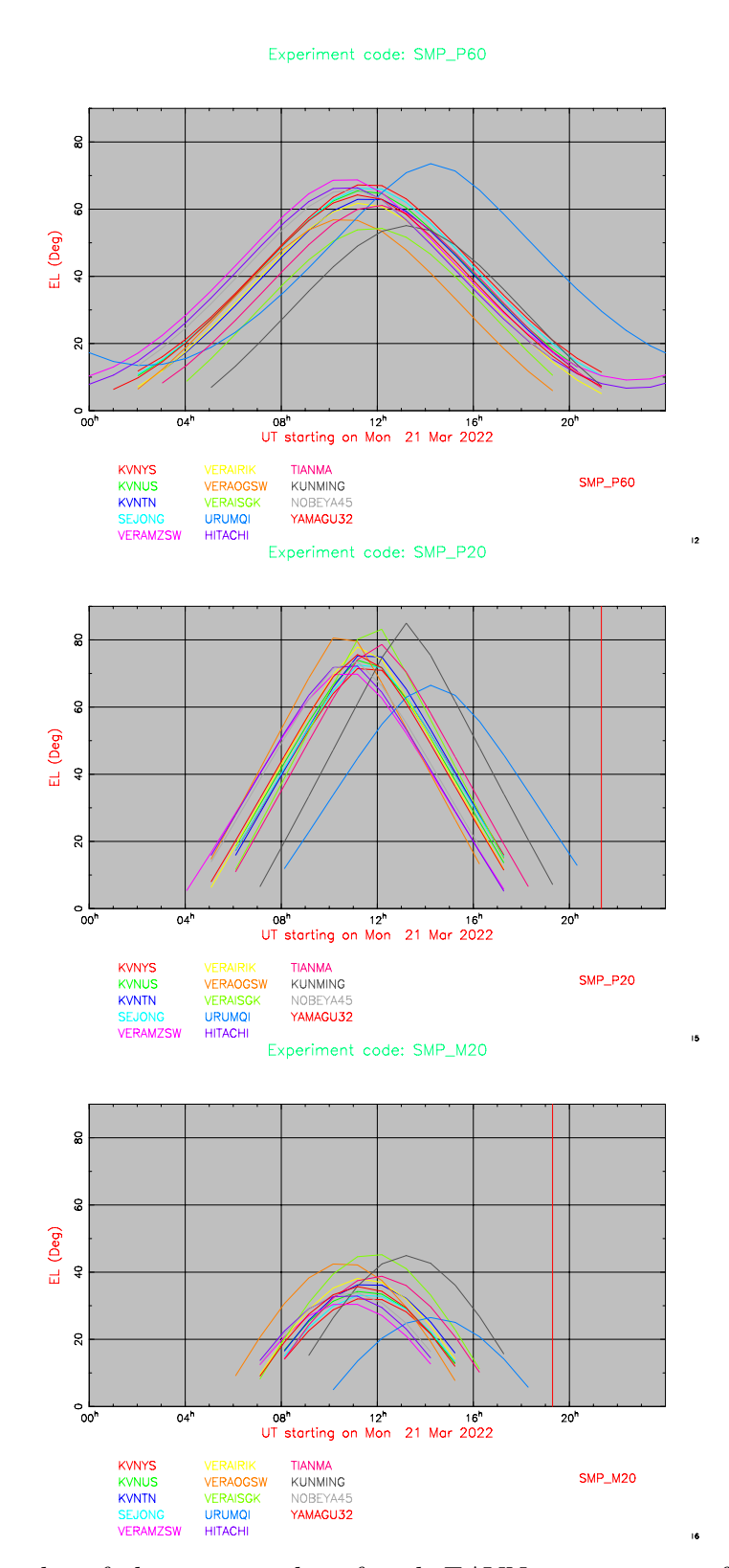


Figure 4: Examples of elevation angles of each EAVN antenna as a function of hour angle for the source's declination of  $+60^{\circ}$  (top panel),  $+20^{\circ}$  (middle panel), and  $-20^{\circ}$  (bottom panel). Note that the elevation angle plot for Sheshan and Takahagi is almost identical to that for Tianma and Hitachi, respectively, because of their positional proximity.

Table 1: Geographic locations and motions of each EAVN antenna.

	) · I				
East	North	Ellipsoidal			
Longitude	Latitude	Height	X	Y	${f Z}$
[°′″]	[° ′ ″]	[m]	[m]	[m]	[m]
138 28 21.2	35 56 40.9	1350	-3871025.4987	3428107.3984	3724038.7361
$140\ 41\ 41.0$	$36\ 41\ 54.5$	117.1	-3961882.0160	3243372.5190	3790687.4570
$140\ 41\ 31.6$	$36\ 41\ 50.8$	120.2	-3961789.1650	3243597.5310	3790597.7000
$131\ 33\ 25.5$	$34\ 12\ 57.7$	133	-3502544.587	3950966.235	3566381.192
$121\ 08\ 09.4$	$31\ 05\ 31.6$	49.2	-2826708.6380	4679237.0440	3274667.5330
$121\ 11\ 58.8$	$31\ 05\ 57.0$	29.4	-2831687.4306	4675733.4626	3275327.4941
$87\ 10\ 40.4$	$43\ 28\ 15.6$	2029.4	228310.1700	4631922.7550	4367064.0740
$102\ 47\ 45.6$	$25\ 01\ 40.8$	1974.0	-1281152.8860	5640864.4013	2682653.4578
$141\ 07\ 57.3$	$39\ 08\ 00.7$	116.6	-3857244.9731	3108782.9179	4003899.1695
$130\ 26\ 23.6$	$31\ 44\ 52.4$	573.6	-3521719.8813	4132174.6817	3336994.1132
$142\ 12\ 59.8$	$27\ 05\ 30.5$	273.1	-4491068.3826	3481545.2394	2887399.8018
$124\ 10\ 15.6$	$24\ 24\ 43.8$	65.1	-3263995.2619	4808056.3902	2619948.6347
$126\ 56\ 27.4$	$37\ 33\ 54.9$	139	-3042281.0183	4045902.6730	3867374.3296
$129\ 14\ 59.3$	$35\ 32\ 44.2$	170	-3287268.6453	4023450.1367	3687379.9886
$126\ 27\ 34.4$	$33\ 17\ 20.9$	452	-3171731.6665	4292678.5393	3481038.7880
$127\ 18\ 11.0$	$36\ 31\ 22.0$	156	-3110079.9600	4082066.7340	3775076.8320
	East Longitude [°'"] 138 28 21.2 140 41 41.0 140 41 31.6 131 33 25.5 121 08 09.4 121 11 58.8 87 10 40.4 102 47 45.6 141 07 57.3 130 26 23.6 142 12 59.8 124 10 15.6 126 56 27.4 129 14 59.3 126 27 34.4	East         North           Longitude         Latitude           [°'"]         35 56 40.9           140 41 41.0         36 41 54.5           140 41 31.6         36 41 50.8           131 33 25.5         34 12 57.7           121 08 09.4         31 05 31.6           121 11 58.8         31 05 57.0           87 10 40.4         43 28 15.6           102 47 45.6         25 01 40.8           141 07 57.3         39 08 00.7           130 26 23.6         31 44 52.4           142 12 59.8         27 05 30.5           124 10 15.6         24 24 43.8           126 56 27.4         37 33 54.9           129 14 59.3         35 32 44.2           126 27 34.4         33 17 20.9	East         North         Ellipsoidal           Longitude         Latitude         Height           [°'"]         [°'"]         [m]           138 28 21.2         35 56 40.9         1350           140 41 41.0         36 41 54.5         117.1           140 41 31.6         36 41 50.8         120.2           131 33 25.5         34 12 57.7         133           121 08 09.4         31 05 31.6         49.2           121 11 58.8         31 05 57.0         29.4           87 10 40.4         43 28 15.6         2029.4           102 47 45.6         25 01 40.8         1974.0           141 07 57.3         39 08 00.7         116.6           130 26 23.6         31 44 52.4         573.6           142 12 59.8         27 05 30.5         273.1           124 10 15.6         24 24 43.8         65.1           126 56 27.4         37 33 54.9         139           129 14 59.3         35 32 44.2         170           126 27 34.4         33 17 20.9         452	$\begin{array}{c ccccccccccccccccccccccccccccccccccc$	East Longitude         North Latitude         Ellipsoidal Height         X         Y           [°'"]         [°'"]         [m]         [m]         [m]           138 28 21.2         35 56 40.9         1350         -3871025.4987         3428107.3984           140 41 41.0         36 41 54.5         117.1         -3961882.0160         3243372.5190           140 41 31.6         36 41 50.8         120.2         -3961789.1650         3243597.5310           131 33 25.5         34 12 57.7         133         -3502544.587         3950966.235           121 08 09.4         31 05 31.6         49.2         -2826708.6380         4679237.0440           121 11 58.8         31 05 57.0         29.4         -2831687.4306         4675733.4626           87 10 40.4         43 28 15.6         2029.4         228310.1700         4631922.7550           102 47 45.6         25 01 40.8         1974.0         -1281152.8860         5640864.4013           141 07 57.3         39 08 00.7         116.6         -3857244.9731         3108782.9179           130 26 23.6         31 44 52.4         573.6         -3521719.8813         4132174.6817           142 12 59.8         27 05 30.5         273.1         -4491068.3826         3481545.2394 <tr< td=""></tr<>

<sup>&</sup>lt;sup>a</sup>The position was measured in late 2016.

Table 2: Station code and average velocity of each KaVA antenna.

Site	$IVS2^a$	$IVS8^b$	$\mathrm{CDP}^c$	$\Delta X [m/yr]^d$	$\Delta Y [m/yr]^d$	$\Delta Z [m/yr]^d$
Mizusawa	Vm	VERAMZSW	7362	-0.0433	-0.0138	-0.0047
Iriki	Vr	VERAIRIK	7364	-0.0159	-0.0049	-0.0098
Ogasawara	Vo	VERAOGSW	7363	0.0363	0.0242	0.0119
Ishigakijima	Vs	VERAISGK	7365	-0.0303	-0.0003	-0.0486
Yonsei	Ky	KVNYONSE		-0.0121	-0.0042	-0.0052
Ulsan	Ku	KVNULSAN		-0.0117	-0.0072	-0.0028
Tamna	$\operatorname{Kt}$	KVNTAMNA		-0.0169	-0.0012	-0.0024

 $<sup>^</sup>a {
m IVS}$  2-characters code

The antenna positions of KVN are regularly monitored by geodetic VLBI observations in collaboration with VERA.

#### 2.2 Antennas

#### 2.2.1 Brief Summary of VERA Antennas

All the telescopes of VERA have the same design, being a Cassegrain-type antenna on AZ-EL mount. Each telescope has a 20 m diameter dish with a focal length of 6 m, and with a sub-reflector of 2.6 m diameter. The dual-beam receiver systems are installed at the Cassegrain focus. Two receivers are set up on the Stewart-mount platforms, which are sustained by steerable six arms, and with such systems one can simultaneously

<sup>&</sup>lt;sup>b</sup>The position was measured in March 2020.

<sup>&</sup>lt;sup>c</sup>The epoch of the coordinate is January 1, 2014.

 $<sup>^{</sup>d}$ The epoch of the coordinates is January 1, 2019.

<sup>&</sup>lt;sup>e</sup>The position was measured in October 2014.

<sup>&</sup>lt;sup>b</sup>IVS 8-characters code

<sup>&</sup>lt;sup>c</sup>CDP (NASA Crustal Dynamics Project) code

<sup>&</sup>lt;sup>d</sup>The epoch of the coordinates is January 01, 2018. Average speed was obtained from the VLBI data from January 01, 2018 to January 1, 2019.

observe two adjacent objects with a separation angle between 0.32 and 2.2 deg. The whole receiver systems are set up on the field rotator (FR), and the FR rotate to track the apparent motion of objects due to the earth rotation. Table 3 summarizes the ranges of elevation (EL), azimuth (AZ) and field rotator angle (FR) with their driving speeds and accelerations. In the case of single beam observing mode, one of two beams is placed at the antenna vertex (separation offset of 0 deg).

#### 2.2.2 Brief Summary of KVN Antennas

The KVN antennas are also designed to be a shaped-Cassegrain-type antenna with an AZ-EL mount. The telescope has a 21 m diameter main reflector with a focal length of 6.78 m. The main reflector consists of 200 aluminum panels with a manufacturing surface accuracy of about 65  $\mu$ m. The slewing speed of the main reflector is 3 °/sec, which enables fast position-switching observations (Table 3). The sub-reflector position, tilt, and tip are remotely controlled and modeled to compensate for the gravitational deformation of the main reflector and for the sagging-down of the sub-reflector itself.

#### 2.2.3 Nobeyama 45-m Telescope

The Nobeyama 45-m Telescope (hereafter NRO45) is one of the largest millimeter radio telescopes in the world. It has a Cassegrain-Coudé optics. The paraboloidal main reflector consists of about 600 pieces of panels, each of which has a surface accuracy of about 60 microns, and the deviation of the whole antenna from an ideal paraboloid is about 90 microns. The sub-reflector has a diameter of 4 m with a convex hyperboloid surface, the position of which is computer-controlled to follow the moving focal point because the main reflector deforms as the elevation angle changes. The slewing speed of the telescope is  $\sim 20^{\circ}$ /min (i.e.,  $0.3^{\circ}$ /sec). The (EL, AZ) driving ranges are also summarized in Table 3. According to the status report of NRO45, observers are required to conduct a pointing measurement and correction every 1 - 1.5 hours. In addition, it is appropriate to conduct a pointing measurement and correction every 30 minutes during the sunrise and sunset when the outside temperature changes drastically. The pointing accuracy above is achievable for wind speed of less than 4 m/s. It can be degraded if a wind velocity exceeds 10 m/s. Users are recommended to avoid observing targets located within 30 degrees from the Sun because the thermal deformation of the antenna degrades the pointing accuracy. Users who would like to observe the Sun or targets near the Sun should take care of them. More details on the NRO45 can be found in the Nobeyama Radio Observatory official website [2].

#### 2.2.4 Takahagi 32-m Telescope

The Takahagi 32-m Telescope (hereafter TAK32) has a shaped Cassegrain-Coude-type design with a 32-m diameter main reflector and a 2.9-m sub-reflector on Az-El mount. The telescope was constructed in 1992. Cryogenically-cooled receivers at 2 frequency bands (6-9 GHz and 21-25 GHz) are equipped. The surface accuracy of the main reflector is < 0.64 mm rms at the antenna elevation angle of 35 deg, and 1.6 mm at other antenna elevation angles. The surface accuracy of the sub-reflector is < 0.2 mm rms. The slewing rates of the main reflector is 0.07 deg/sec, as shown in Table 3. The

tentative value of aperture efficiency of TAK32 is 30% at K-band (see Table 4; [19]). Although TAK32 can point to the El range of  $5^{\circ} \leq El \leq 88^{\circ}$ , we recommend to use at the El range of  $15^{\circ} \leq El \leq 85^{\circ}$  because the pointing accuracy is not secured at  $El \leq 15^{\circ}$ .

#### 2.2.5 Hitachi 32-m Telescope

The Hitachi 32-m Telescope (hereafter HIT32) has a shaped Cassegrain-Coude-type design with a 32-m diameter main reflector and a 2.9-m sub-reflector on Az-El mount. The telescope was constructed in 1983. Cryogenically-cooled receivers at 2 frequency bands (6 – 9 GHz and 21 – 25 GHz) are equipped. The surface accuracy of the main reflector is < 0.64 mm rms at the antenna elevation angle of 35 deg, and 1.6 mm at other antenna elevation angles. The surface accuracy of the sub-reflector is < 0.2 mm rms. The slewing rates of the main reflector is 0.2 deg/sec, as shown in Table 3. The value of aperture efficiency of HIT32 is 60–75% at C-band (see Table 4; [19]). Although HIT32 can point to the El range of  $5^{\circ} \leq El \leq 88^{\circ}$ , we recommend to use at the El range of  $15^{\circ} \leq El \leq 85^{\circ}$  because the pointing accuracy is not secured at  $El \leq 15^{\circ}$ .

#### 2.2.6 Yamaguchi 32-m Telescope

The Yamaguchi 32-m Telescope (hereafter YAM32) has a shaped Cassegrain-Coude-type design with a 32-m diameter main reflector and a 2.9-m sub-reflector on Az-El mount. The telescope was constructed in 1979. A cryogenically-cooled receiver for 6 and 8 GHz observation is equipped. The surface accuracy of the main reflector is < 0.64 mm rms at the antenna elevation angle of 35 deg, and 1.6 mm at other antenna elevation angles. The surface accuracy of the sub-reflector is < 0.2 mm rms. The slewing rates of the main reflector is 0.25 deg/sec, as shown in Table 3. The value of aperture efficiency of YAM32 is 60–70% at C-band (see Table 4).

#### 2.2.7 Tianma 65-m Telescope

The Tianma 65-m Telescope (hereafter TMRT65) has a shaped Cassegrain-type design with a 65-m diameter main reflector and a 6.5-m sub-reflector on Az-El mount. The main reflector consists of 1008 aluminum panels deploying an active surface control system with 1104 actuators. The prime mirror achieves a surface accuracy of about 0.3 mm rms after compensating the gravitational deformation in real time by the active surface control system. The secondary mirror has a surface error of 0.1 mm rms. A rotatable receiver cabin with the feeds covering frequency range from S-band (2 GHz) to Q-band is mounted at the Cassegrain focus, while the L-band (1.6 GHz) feed is off focus mount separately. The slewing rates of the main reflector are 0.5°/sec in azimuth and 0.3°/sec in elevation, as shown in Table 3. An overhead time of 10 seconds is recommended to settle the antenna on source.

Dual-beam receivers are installed in TMRT65 at both K- and Q-bands. These two beams have a fixed separation angle of 140 arcsec at K-band and 100 arcsec at Q-band. One of the beams is placed at the antenna focus for VLBI observations. The measured beam sizes (HPBW) are listed in Table 4.

#### 2.2.8 Sheshan 25-m Telescope

The Sheshan 25-m Telescope (hereafter SHRT25) is a Cassegrain-type beam wave-guide antenna. The telescope has been in operation since 1987 and is located  $\sim 6.1$  kilometers from TMRT65. Current receiver system include a room-temperature C-band (6.7 GHz) receiver and a cooled S/X co-axis feed receiver. The main surface accuracy is 0.65 mm rms. The slewing speed are  $1.0^{\circ}/\text{sec}$  in azimuth and  $0.6^{\circ}/\text{sec}$  in elevation, as shown in Table 3.

#### 2.2.9 Nanshan 26-m Telescope

The Nanshan 26-m Telescope (hereafter NSRT26) has a Cassegrain-type design with a 26-m diameter main reflector and a 3-m sub-reflector on Az-El mount. The telescope was constructed in 1993 with 25-m-diameter main reflector, while refurbishment of the telescope was completed in 2015 resulting in enlargement of the main reflector of 26 m and improvement of the antenna surface accuracy. Receivers at five frequency bands, L, S/X, C, K, and Q, are equipped, while the new Q-band cooled receiver had been installed in 2018 and now is under evaluation. The surface accuracy of main- and sub-reflectors are 0.4 mm rms and 0.1 mm rms, respectively. The slewing rates of the main reflector are 1.0°/sec in azimuth and 0.5°/sec in elevation, as shown in Table 3.

#### 2.2.10 Kunming 40-m Telescope

The Kunming 40-m Telescope (hereafter KMRT40) has a Cassegrain-type design with a 40-m diameter main reflector and a 4.2-m sub-reflector on Az-El mount. The main reflector which diameter within 26 meters is solid aluminum panel and 26 to 40 meters is stainless steel mesh. The telescope was constructed in 2006 with only S/X receivers and upgraded in 2016 for installing a C-band receiver (4–8 GHz). The surface accuracy of solid aluminum panel and stainless steel mesh are 0.5 mm rms and 2.5 mm rms, respectively. The slewing rates of the main reflector are 1.0°/sec in azimuth and 0.5°/sec in elevation, as shown in Table 3.

#### 2.2.11 Sejong 22-m Telescope

The Sejong Telescope (hereafter KSJ) is a Cassegrain-type 22-m diameter telescope built primarily for geodetic research, and can be observed at S, X, K and Q bands. Among them, S/X bands were designed for observation with the International VLBI Service (IVS), while K- and Q bands were designed for astronomical observation. The slewing speed of the antenna is  $\sim 5^{\circ}/\text{sec}$  in both azimuth and elevation, which enables fast position-switching observations (see Table 3). Like KVN telescopes, the subreflector position, tilt, and tip are remotely controlled and modeled to compensate for the gravitational deformation of the main reflector and for the sagging-down of the subreflector itself. The pointing accuracy is  $\sim 3''$  and 5'' in the azimuth and elevation, respectively.

Table 3: Driving performance of EAVN telescopes.

		ving periormance or	-
Driving axis	Driving range	Max. driving speed	Max. driving acceleration
		Nobeyama	
$\overline{\mathrm{AZ}^a}$	$-75^{\circ} \sim 435^{\circ}$	$0.3^{\circ}/\mathrm{sec}$	$0.3^{\circ}/\mathrm{sec}^2$
$\operatorname{EL}$	$12^{\circ} \sim 80^{\circ}$	$0.3^{\circ}/\mathrm{sec}$	$0.3^{\circ}/\mathrm{sec^2}$
		Takahagi	
$\mathrm{AZ}^a$	$11^{\circ} \sim 349^{\circ}$	$0.07^{\circ}/\mathrm{sec}$	$0.035^{\circ}/\mathrm{sec}^2$
$\operatorname{EL}$	$5^{\circ} \sim 88^{\circ c}$	$0.07^{\circ}/\mathrm{sec}$	$0.035^{\circ}/\mathrm{sec^2}$
		Hitachi	·
$\mathrm{AZ}^a$	$2^{\circ} \sim 358^{\circ}$	$0.2^{\circ}/\mathrm{sec}$	$0.12^{\circ}/\mathrm{sec}^2$
$\operatorname{EL}$	$5^{\circ} \sim 88^{\circ c}$	$0.2^{\circ}/\mathrm{sec}$	$0.12^{\circ}/\mathrm{sec}^2$
		Yamaguchi	·
$-$ AZ $^a$	$2^{\circ} \sim 358^{\circ}$	$0.25^{\circ}/\mathrm{sec}$	$0.5^{\circ}/\mathrm{sec}^2$
$\operatorname{EL}$	$5^{\circ} \sim 85^{\circ}$	$0.25^{\circ}/\mathrm{sec}$	$0.5^{\circ}/\mathrm{sec}^2$
		Tianma	·
$-$ AZ $^a$	$-60^{\circ} \sim 425^{\circ}$	$0.5^{\circ}/\mathrm{sec}$	$0.27^{\circ}/{\rm sec^2}$
$\operatorname{EL}$	$8^{\circ} \sim 88^{\circ}$	$0.3^{\circ}/\mathrm{sec}$	$0.16^{\circ}/\mathrm{sec}^2$
		Sheshan	,
$-$ AZ $^a$	$-78^{\circ} \sim 430^{\circ}$	1.0°/sec	$0.5^{\circ}/\mathrm{sec}^2$
$\operatorname{EL}$	$5^{\circ} \sim 88.5^{\circ}$	$0.6^{\circ}/\mathrm{sec}$	$0.28^{\circ}/\mathrm{sec}^2$
		Nanshan	,
$-$ AZ $^a$	$-270^{\circ} \sim 270^{\circ}$	$1.0^{\circ}/\mathrm{sec}$	$0.5^{\circ}/\mathrm{sec}^2$
$\operatorname{EL}$	$5^{\circ} \sim 88^{\circ}$	$0.5^{\circ}/\mathrm{sec}$	$0.5^{\circ}/\mathrm{sec^2}$
-		Kunming	·
$-$ AZ $^a$	$-270^{\circ} \sim 270^{\circ}$	$1.0^{\circ}/\text{sec}$	$0.3^{\circ}/\mathrm{sec^2}$
$\operatorname{EL}$	$8^{\circ} \sim 88^{\circ}$	$0.5^{\circ}/\mathrm{sec}$	$0.3^{\circ}/\mathrm{sec^2}$
		VERA	,
$-$ AZ $^a$	$-90^{\circ} \sim 450^{\circ}$	2.1°/sec	$2.1^{\circ}/\mathrm{sec}^2$
$\operatorname{EL}$	$5^{\circ} \sim 85^{\circ}$	$2.1^{\circ}/\mathrm{sec}$	$2.1^{\circ}/\mathrm{sec}^2$
$\mathrm{FR}^b$	$-270^{\circ} \sim 270^{\circ}$	$3.1^{\circ}/\mathrm{sec}$	$3.1^{\circ}/\mathrm{sec}^2$
		KVN	,
$-$ AZ $^a$	$-90^{\circ} \sim 450^{\circ}$	$3.0^{\circ}/\mathrm{sec}$	$3.0^{\circ}/\mathrm{sec}^2$
$\operatorname{EL}$	$5^{\circ} \sim 85^{\circ}$	$3.0^{\circ}/\mathrm{sec}$	$3.0^{\circ}/\mathrm{sec}^2$
		Sejong	,
$-$ AZ $^a$	$-270^{\circ} \sim 270^{\circ}$	5.0°/sec	$5.0^{\circ}/\mathrm{sec}^2$
$\operatorname{EL}$	$0^{\circ} \sim 90^{\circ}$	$5.0^{\circ}/\mathrm{sec}$	$5.0^{\circ}/\mathrm{sec}^2$
			<u>'</u>

<sup>&</sup>lt;sup>a</sup>The north is  $0^{\circ}$  and the east is  $90^{\circ}$ .

#### 2.2.12 Aperture Efficiency

The aperture efficiency of each VERA antenna is 50–55% at C-band, and about 40–50% at both K- and Q-bands (see Table 4). The measurements at C-band were based on the observations of 3C274 and Cyg-A (3C405) assuming that the flux densities are 58.7 and 237.4 Jy in C-band [16], respectively. For the K- and Q-bands, Jupiter is used for aperture efficiency measurements assuming the brightness temperature of 160 K in both K- and Q-bands. Due to the bad weather condition in some of the sessions, the measured efficiencies show large scatter. However, we conclude that the aperture efficiencies are not significantly changed compared with previous measurements. The elevation dependence of aperture efficiency for VERA antenna was also measured from the observations toward Cyg-A (3C405) and maser sources at C-band and K/Q-bands, respectively. Figure 5 (bottom-right panel) shows the relations between the elevation

<sup>&</sup>lt;sup>b</sup>Field rotator. FR is 0° when Beam-1 is at the sky side and Beam-2 is at the ground side, and CW is positive when a telescope is seen from a target source.

 $<sup>^</sup>c$ Recommended EL range is  $15^\circ$ – $85^\circ$  for the Takahagi and Hitachi antennas.

Table 4: Aperture efficiency, beam size, and DPFU<sup>a</sup> of EAVN telescopes.

		C-1	C-band (6.7 GHz)			-band (22	GHz)	Q	Q-band (43 GHz)		
Telescope	D	$\overline{\eta_{ m A}}$	HPBW	DPFU	$\overline{\eta_{ m A}}$	HPBW	DPFU	$\overline{\eta_{ m A}}$	HPBW	DPFU	
Name	(m)	(%)	(arcsec)	(K/Jy)	(%)	(arcsec)	(K/Jy)	(%)	(arcsec)	(K/Jy)	
Nobeyama	45	_	_	_	61	72	0.351	53	39	0.305	
Takahagi	32	—	_		30	100	0.087		_	_	
Hitachi	32	60 - 75	270 - 280	0.197	_	_		_		_	
Yamaguchi	32	60 - 70	310	0.197	_	_		_		_	
Tianma	65	50 – 55	140	0.631	50	44	0.601	45	22	0.541	
Nanshan	26		_	_	60	115	0.115	_		_	
Sheshan	25	40 – 42	370	0.073	_	_		_		_	
$\operatorname{Kunming}^b$	40	20 – 30	282	0.121	_	_		_		_	
Mizusawa	20	50 – 55	530	0.060	48	139	0.055	50	74	0.057	
Iriki	20	50 – 55	510	0.060	44	147	0.050	40	74	0.046	
Ogasawara	20	50 – 55	515	0.060	43	142	0.049	42	74	0.048	
Ishigakijima	20	50 – 55	530	0.060	44	142	0.050	42	72	0.048	
Yonsei	21		_	_	55	127	0.069	63	63	0.079	
Ulsan	21	62	420	0.078	63	124	0.079	61	63	0.077	
Tamna	21		_	_	60	126	0.075	63	63	0.079	
Sejong	22				59	120	0.081	53	60	0.073	

<sup>&</sup>lt;sup>a</sup>: Degree Per Flux density Unit.

and the aperture efficiency measured for VERA Iriki station at K/Q-bands, while Figure 6 shows the same relation measured via integrating all the VERA stations data in C-band. The aperture efficiency at low elevation of  $\leq 30$  deg increases slightly in C-band, while  $\leq 20$  deg decreases slightly in K/Q-bands. However, possible changes in the efficiency is less than about 20% and 10% at C- and K/Q-bands, respectively. Concerning this elevation dependence, the observing data FITS file include a gain curve table (GC table), which is AIPS readable, in order to calibrate the dependence when the data reduction.

The aperture efficiency and beam size for each KVN antenna are also listed in Table 4. Aperture efficiency of KVN varies with elevation as shown in Figure 5. The main reflector panels of KVN antennas were installed to give the maximum gain at the elevation angle of 48°. The sagging of sub-reflector and the deformation of main reflector by gravity with elevation results in degradation of antenna aperture efficiency with elevation. In order to compensate this effect, KVN antennas use a hexapod to adjust sub-reflector position. Figure 5 shows the elevation dependence of antenna aperture efficiency of the KVN 21 m radio telescopes measured by observing Venus or Jupiter. By fitting a second order polynomial to the data and normalizing the fitted function with its maximum, we derived a normalized gain curve which has the following form:

$$G_{\text{norm}} = A_0 E L^2 + A_1 E L + A_2,$$
 (1)

where EL is the elevation in degree.

Aperture efficiency and beam size for non-KaVA telescopes are also summarized in Table 4. The values for NRO45 are based on the latest measurements in autumn 2017, where the Jupiter or the Mars was used as a reference source. The elevation dependence of the aperture efficiency is approximately constant over a range of El  $\sim 25^{\circ}$  –  $50^{\circ}$  at both K- and Q-bands.

In TMRT65, the main reflector panels were assembled to give the maximum surface

<sup>&</sup>lt;sup>b</sup>: Low  $\eta_A$  due to problems with the feed, fixing.

accuracy at the elevation angle of  $52^{\circ}$ . The aperture efficiency goes down to less than 10% at low ( $< 10^{\circ}$ ) and high ( $> 80^{\circ}$ ) elevation angles, mainly due to the gravitational deformation. The active surface control system is used for compensating the gravitational effect at different elevation angles, making the gain curves as a constant over the elevation. Figure 7 shows the elevation dependence of the aperture efficiency at Q-band with or without the active surface control. The active surface control system is set 'ON' by default at K- and Q-band observations. To calibrate visibility amplitude, conversion factors from temprature (in unit of K) to flux density (in unit of Jy) are required. These factors, DPFU (Degree Per Flux density Unit), are also summarized in Table 4.

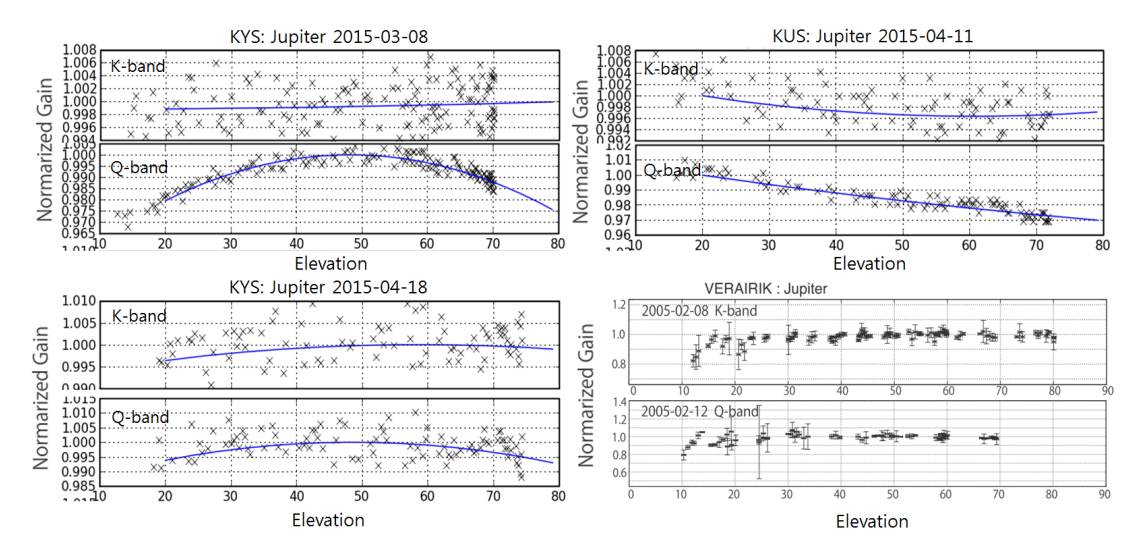


Figure 5: The elevation dependence of the aperture efficiency for KVN three antennas and VERA Iriki antenna. For KVN antennas, the maximum gain is given at the elevation angle of  $48^{\circ}$ . The efficiency in K-band (on Feb 8, 2005) and the Q-band (on Feb 12, 2005) for VERA Iriki antenna is shown in *bottom right*. The efficiency is relative value to the measurement at EL =  $50^{\circ}$ .

#### 2.2.13 Beam Pattern and Size

Figure 8 upper panels shows the beam patterns for VERA at K-band. The side-lobe level is less than about -15 dB, except for the relatively high side-lobe level of about -10 dB for the separation angle of 2.0 deg at Ogasawara station. The side-lobe of the beam patterns has an asymmetric shape, but the main beam has a symmetric Gaussian shape without dependence on separation angle. Figure 9 shows the beam patterns for VERA Mizusawa and Ishigakijima stations at C-band (single-beam mode) measured via observing strong CH<sub>3</sub>OH maser sources G 009.62+00.196 and W3-IRS5, which can be assumed as a point source, on 2017 Apr 5-8. Almost the similar side-lobe pattern is clearly seen in both stations and other VERA two stations as well. The measured beam sizes (HPBW) in C-, K- and Q-bands based on the data of the pointing calibration are also summarized in Table 4. The main beam sizes show no dependence on the dual-beam separation angle.

The optics of KVN antenna is a shaped Cassegrain type of which the main reflector and subreflector are shaped to have a uniform illumination pattern on an aperture

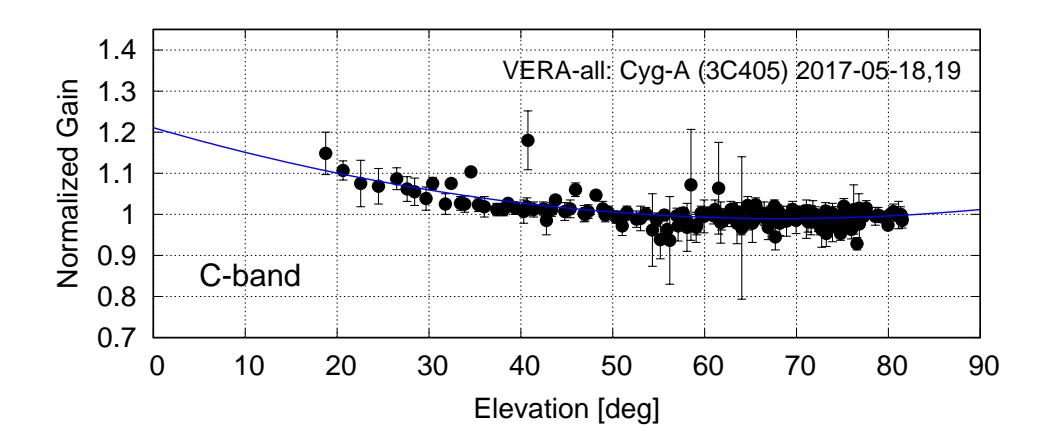


Figure 6: The elevation dependence of the aperture efficiency for VERA in C-band. This gain curve was measured on May 18 and 19, 2017 via observing Cyg-A (3C405) and integrating all the VERA stations data. The efficiency in this plot is relative value to the measurement at  $EL = 50^{\circ}$ .

plane. Because of the uniform illumination, KVN antennas can get higher aperture efficiency than value of typical Cassegrain type antenna. However, higher side-lobe level is inevitable. OTF images of Jupiter at K- and Q-bands are shown in Figure 8. The map size is  $12' \times 10'$  and the first side-lobe pattern is clearly visible. Typical side-lobe levels of KVN antennas are 13-14 dB.

#### 2.3 Receivers

#### 2.3.1 Brief Summary of VERA Receiving System

Each VERA antenna has the receivers for 5 bands, which are S (2 GHz), C (6.7 GHz), X (8 GHz), K (22 GHz), and Q (43 GHz) bands. For the open use, C-band, K-band and Q-band are open for observation. The low-noise HEMT amplifiers in the K- and Q-bands are enclosed in the cryogenic dewar, which is cooled down to 20 K, to reduce the thermal noise. On the other hand, both the amplifier and polarizer in C-band are operated at room temperatures. The range of observable frequency and the typical receiver noise temperature  $(T_{\rm RX})$  at each band are summarized in Table 5 and Figure 10.

After the radio frequency (RF) signals from astronomical objects are amplified by the receivers, the RF signals are mixed with standard frequency signal generated in the first local oscillator to down-convert the RF to an intermediate frequency (IF) of  $4.7~\mathrm{GHz}-7~\mathrm{GHz}$ . The first local frequencies are fixed at  $16.8~\mathrm{GHz}$  in K-band and at  $37.5~\mathrm{GHz}$  in Q-band. The IF signals are then mixed down again to the base band frequency of  $0-512~\mathrm{MHz}$ . The frequency of second local oscillator is tunable with a possible frequency range between 4 GHz and 7 GHz. The correction of the Doppler effect due to the earth rotation is carried out in the correlation process after the observation. Therefore, basically the second local oscillator frequency is kept to be constant during the observation. Figure 11 shows a flow diagram of these signals for VERA.

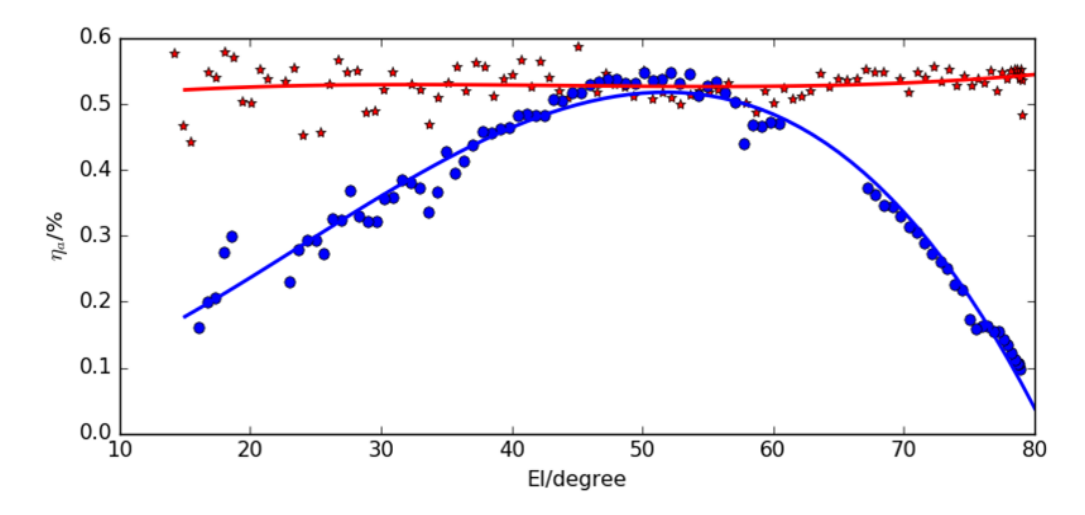


Figure 7: Elevation dependence of the aperture efficiency ( $\eta_{\text{eff}}$ ) for TMRT65 at Q-band. The red and blue colors represent  $\eta_{\text{eff}}$  with or without the active surface control, respectively.

Figure 8: **EPS** files are tentatively removed to avoid compile error (Timeout): The beam patterns in the K-band for VERA (A-beam) Iriki with the separation angle of  $0^{\circ}$  (*Upper left*) and Ogasawara with the separation angle of  $2.0^{\circ}$  (*Upper right*), and in K/Q-band for KVN Yonsei. The patterns of VERA antennas were derived from the mapping observation of strong H<sub>2</sub>O maser toward W49N, which can be assumed as a point source, with grid spacing of 75". In the case of KVN antennas, the patterns were derived from the OTF images of Venus at K/Q-band.

#### 2.3.2 Brief Summary of KVN Receiving System

The KVN quasi-optics are uniquely designed to observe 22, 43, 86 and 129 GHz band simultaneously [7], [8]. Figure 12 shows the layout of quasi-optics and receivers viewing from sub-reflector side. The quasi-optics system splits one signal from sub-reflector into four using three dichroic low-pass filters marked as LPF1, LPF2 and LPF3 in the Figure 12. The split signals into four different frequency bands are guided to corresponding receivers.

Figure 13 shows a signal flows in KVN system. The 22, 43 and 86 GHz band receivers are cooled HEMT receivers and the 129 GHz band receiver is a SIS mixer receiver. All

Figure 9: **EPS** files are tentatively removed to avoid compile error (Timeout): The beam patterns in C-band for VERA antennas (single beam) at Mizusawa and Ishigakijima stations. The patterns were derived from the mapping observation of strong CH<sub>3</sub>OH masers toward G 009.62+00.196 and W3-IRS5, which can be assumed as a point source, with grid spacing of 4' in  $56' \times 56'$  field. These observations were done in Apr 5–8, 2017.

Table 5: Frequency range and  $T_{RX}$  of receivers at each EAVN telescope.

	Frequency Range	$\frac{dT_{\rm RX}}{T_{\rm RX}}^a$	Polarization
	[GHz]	[K]	
		Nobeyama	
K	21.5 - 23.8	$\sim 85$	LCP/RCP
Q	42.5 - 44.5	$\sim 111$	LCP
		Takahagi	
K	21.0 - 25.0	$\sim 30$	LCP/RCP
		Hitachi	
С	6.6 - 7.1	$\sim 20$	LCP/RCP
		Yamaguchi	
С	6.6 - 7.1	18	LCP/RCP
		Tianma	
$\overline{C}$	4.0 - 8.0	$\sim 20$	LCP/RCP
K	18.0 - 26.5	16 - 35	LCP/RCP
Q	39 - 47	35 - 50	LCP/RCP
		Nanshan	
K	22.0 - 24.2	$\sim 15$	LCP/RCP
Q		(under evaluation)	
		Sheshan	
С	5.975 - 6.825	~ 100	LCP/RCP
		Kunming	
С	4.0 - 8.0	$\sim 20$	LCP/RCP
		VERA	
С	6.3 - 7.0	80 - 100	LCP
K	21.5 - 23.8	30 - 50	$LCP^c$
Q	42.5 - 44.5	70 - 90	LCP
		KVN	
$C^{b}$	6.3 - 7.0	~ 300	LCP
K	18 - 26	20 - 40	LCP/RCP
Q	35 - 50	40 - 50 (Yonsei)	LCP/RCP
	42.11 - 44.11	40 - 50  (Ulsan)	LCP/RCP
	42.11 - 44.11	70 - 80  (Tamna)	LCP/RCP
		Sejong	
K	21.4 - 23.1	$\sim 31$	LCP/RCP
Q	42.3 - 43.9	$\sim 86$	LCP/RCP

<sup>&</sup>lt;sup>a</sup> Receiver noise temperature.

receivers can receive dual-circular-polarization signals. Among eight signals (four dual-polarization signals), four signals selected by the IF selector are down-converted to the input frequency band of the sampler. The instantaneous bandwidth of the 1st IF of each receiver is limited to 2 GHz by the band-pass filter. The 1st IF signal is down-converted by BBCs to the sampler input frequency ( $512-1024~\mathrm{MHz}$ ) band.

Typical noise temperatures of K- and Q-bands are presented in Table 5. Since the calibration chopper is located before the quasi-optics as shown in Figure 12, the loss of quasi-optics contributes to receiver noise temperature instead of degrading antenna aperture efficiency. Therefore, the noise temperature in the table includes the contribution due to the quasi-optics losses.

<sup>&</sup>lt;sup>b</sup> Only for the Ulsan antenna.

 $<sup>^{</sup>c}$  RCP is used for the simultaneous K/Q band mode (see Section 4.4).

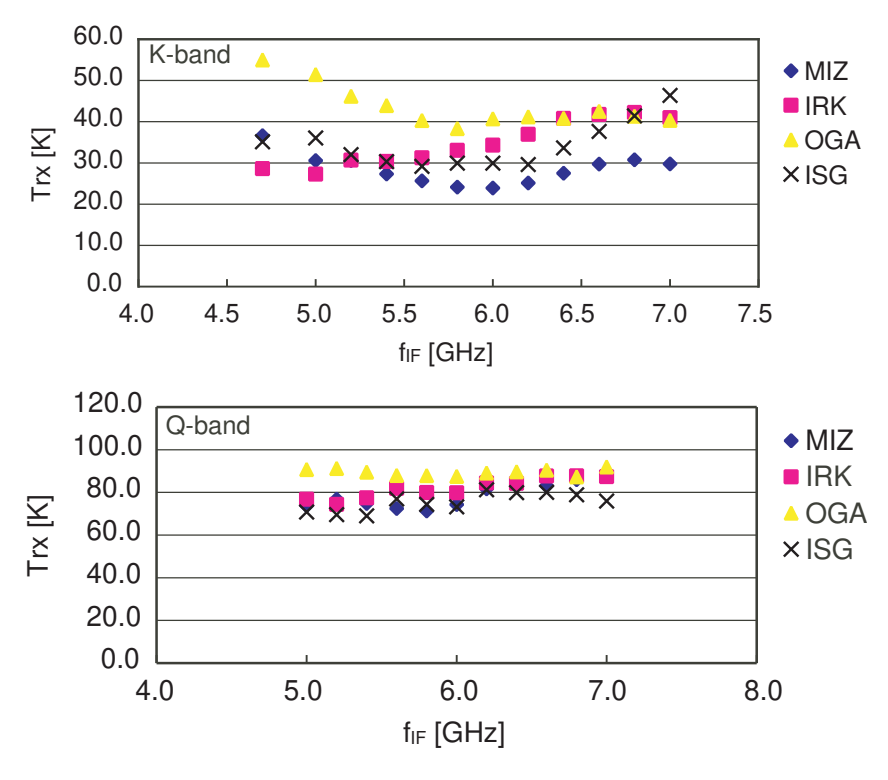


Figure 10: Receiver noise temperature for each VERA antenna. Top and bottom panels show measurements in the K- and Q-bands, respectively. Horizontal axis indicate an IF (intermediate frequency) at which  $T_{\rm RX}$  is measured. To convert it to RF (radio frequency), add 16.8 GHz in K-band and 37.5 GHz in Q-band to the IF frequency.

#### 2.3.3 Brief Summary of NRO45 Receiving System

The NRO45 covers an observing frequency range of 20-116 GHz with multiple receivers. The VLBI backend system of the NRO45 is currently equipped at K-band and Q-band. Figure 14 illustrates a flow diagram of the VLBI receiving system in the NRO45. The observable RF range and typical receiver noise temperature for the receivers at K- and Q-bands are also summarized in Table 5. The received RF signals are down-converted into an IF range of 5-7 GHz, then the IF signals are mixed down to the another IF range of 400-2000 MHz, and finally filtered to the base bands of 512-1024 MHz and 1024-1536 MHz in K- and Q-bands, respectively, which are the inputs to the A/D sampler.

Currently, one of the receivers can be selected by switching the mirrors in the optics in a few minutes manually. Since 2020B, K- and Q-band observations can be conducted simultaneously by inserting a perforated high-pass dichroic plate. When using the dichroic plate, the gain of the Q-band signals may be reduced by 0.3 dB (in 2018 June), causing the rise of the system noise temperature by about 30 K in Q-band.

#### 2.3.4 Brief Summary of TAK32 Receiving System

Figure 15 shows a flow diagram of the VLBI receiving system in TAK32. TAK32 covers an observing frequency range of 6-9 GHz and 21-25 GHz with two cryogenically-cooled receivers, while TAK32 joins in EAVN observations at only K-band in the 2022A

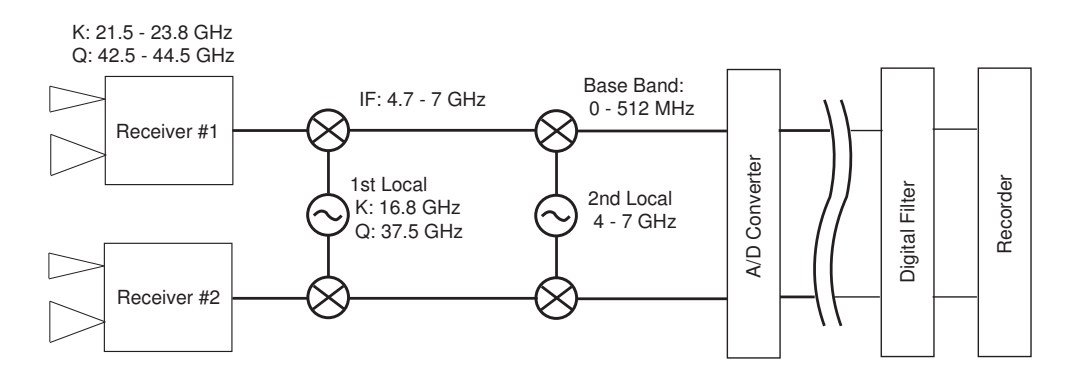


Figure 11: Flow diagram of signals from receiver to recorder for VERA.

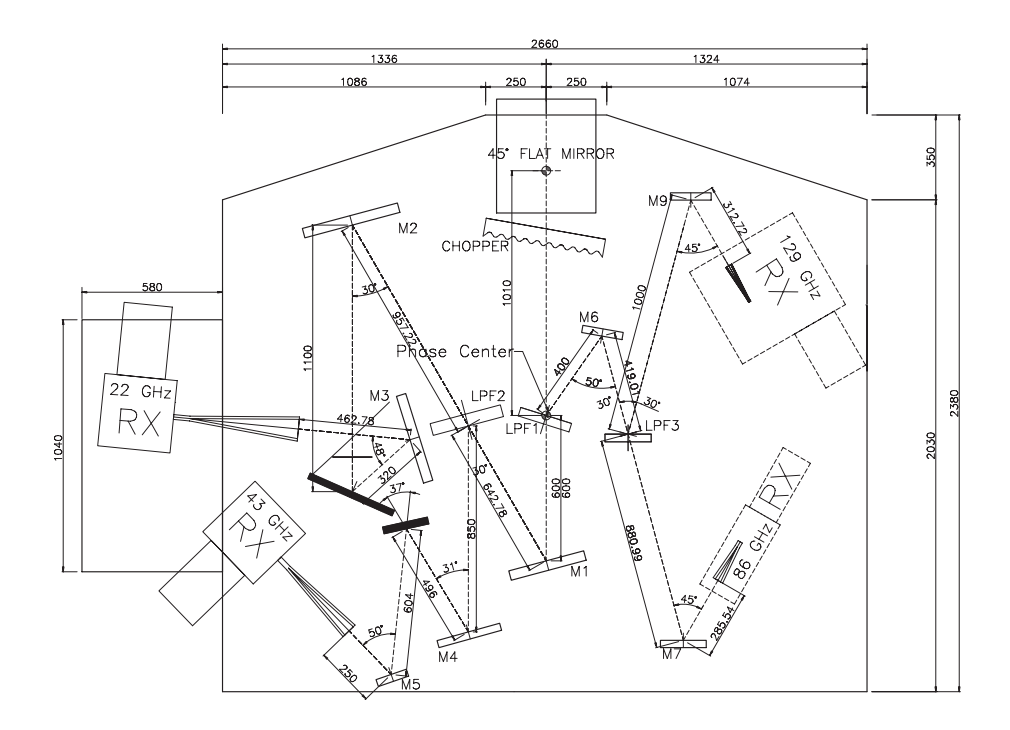


Figure 12: KVN multi-frequency receiving system [7], [8].

#### semester.

The flow diagram of TAK32 is shown in Figure 15. The K-band receiver is cooled with dual circular polarization. The observable frequency range and the typical receiver noise temperature are shown in Table 5. The total system noise temperatures at K-band is typically 40 K at winter with good weather, > 100 K at winter with bad weather, 150 K at summer with good weather, and > 500 K at summer with bad weather.

For K-band, received RF signals are down-converted into an IF range of 8.0-8.8 GHz, and the IF signals are then mixed down to the base band of 512-1024 MHz, which is the input to the A/D sampler ADS-3000+. The data with the rate of 1024 MHz  $\times$  2 bit are recorded by OCTADISK, and then the digital base-band converter is used to convert the 2 Gbps data into 1 Gbps.

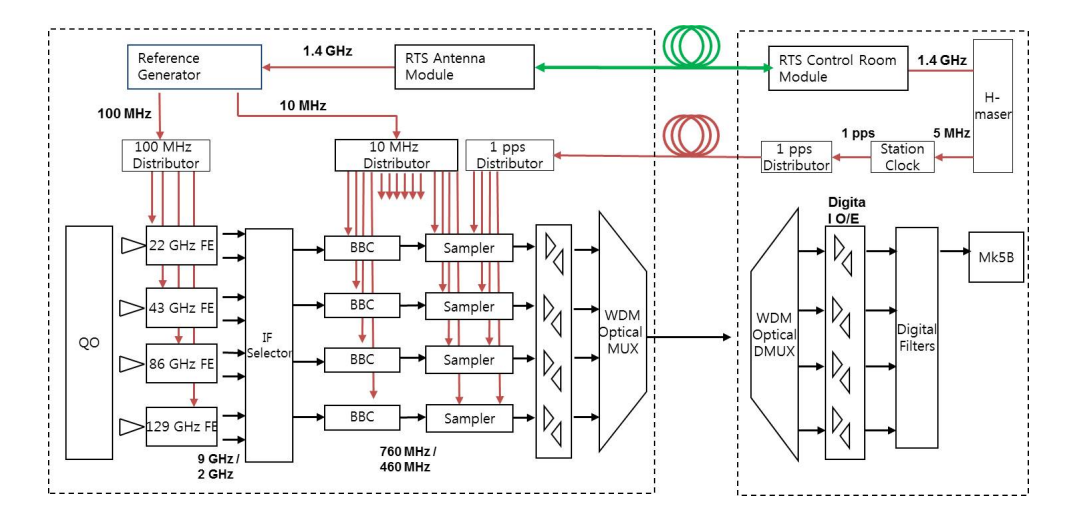


Figure 13: Flow diagram of signals from receiver to recorder for KVN [15].

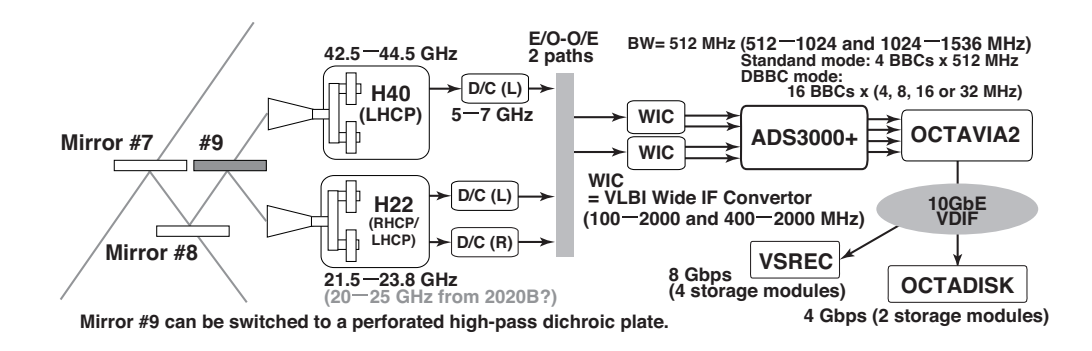


Figure 14: Flow diagram of signals from receiver to recorder for NRO45.

#### 2.3.5 Brief Summary of HIT32 Receiving System

Figure 16 shows a flow diagram of the VLBI receiving system in HIT32. HIT32 covers an observing frequency range of 6-9 GHz and 21-25 GHz with two cryogenically-cooled receivers, while HIT32 joins in EAVN observations at only C-band in the 2022A semester.

The flow diagram of HIT32 is shown in Figure 16. The C-band receiver is cooled with dual circular polarization. The observable frequency range and the typical receiver noise temperature are shown in Table 5. The total system noise temperatures at C-band is typically 30 K with good weather and  $\sim 40$  K with bad weather.

For C-band, received RF signals are mixed down to the base band of 512-1024 MHz, which is the input to the A/D sampler ADS-3000+. The data with the rate of 1024 MHz  $\times$  2 bit are recorded by OCTADISK, and then the digital base-band converter is used to convert the 2 Gbps data into 1 Gbps.

#### 2.3.6 Brief Summary of YAM32 Receiving System

The flow of the VLBI receiving system in YAM32 is the same with that of HIT32. YAM32 covers an observing frequency range of 6 – 9 GHz with a cryogenically-cooled receivers, while YAM32 joins in EAVN observations at only C-band in the 2022A

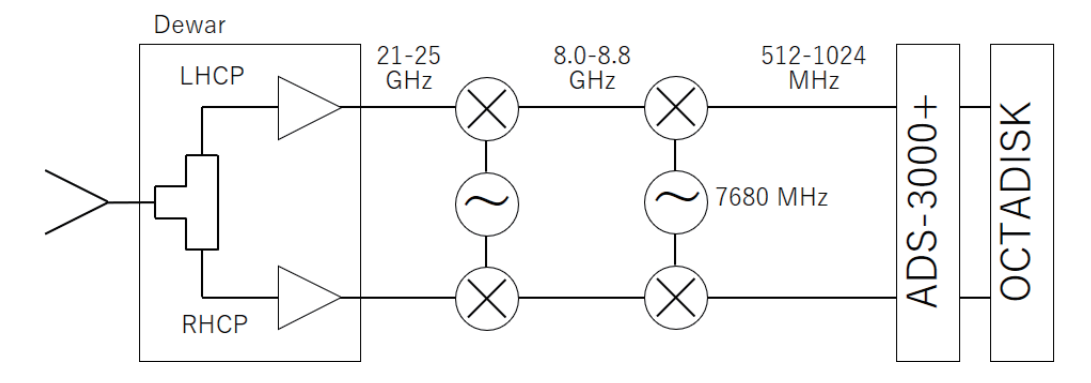


Figure 15: Flow diagram of signals from receiver to recorder for TAK32.

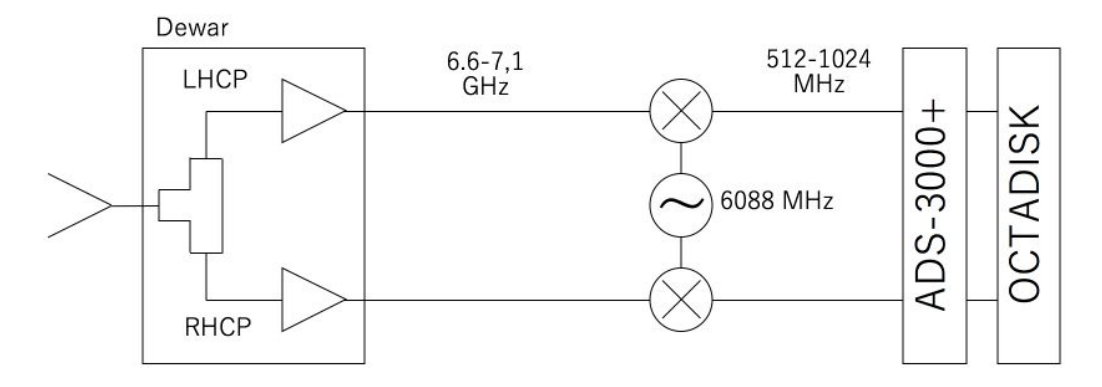


Figure 16: Flow diagram of signals from receiver to recorder for HIT32.

semester.

The C-band receiver is cooled with dual circular polarization. The observable frequency range and the typical receiver noise temperature are shown in Table 5. The total system noise temperatures at C-band is typically 50 K with good weather and  $\sim 80~\rm K$  with bad weather.

For C-band, received RF signals are mixed down to the base band of 512-1024 MHz, which is the input to the A/D sampler ADS-3000+. The data with the rate of 1024 MHz  $\times$  2 bit are recorded by OCTADISK, and then the digital base-band converter is used to convert the 2 Gbps data into 1 Gbps.

#### 2.3.7 Brief Summary of TMRT65 Receiving System

Figure 17 shows a flow diagram of the VLBI receiving system in TMRT65. TMRT65 has the receivers for 8 frequency bands, L (1.4 GHz), S/X (2.3/8.4 GHz), C (6.7 GHz), X/Ka (8.4/31.0 GHz), Ku (15 GHz), K (22 GHz), and Q (43 GHz). The K- and Q-band receivers are cooled HEMT receivers with dual circular polarizers. The observable frequency range and the typical receiver noise temperature are shown in Table 5. The total system noise temperatures at K- and Q-bands are typically 70 and 110 K, respectively. The RF signal is firstly down-converted to IF range of 4 – 12 GHz and it is transferred by optical fibers to the observing room, where the signal is further down-converted to 0 – 1024 MHz (actually in 10 – 512 MHz and 512 – 1024 MHz) at the input of BBCs.

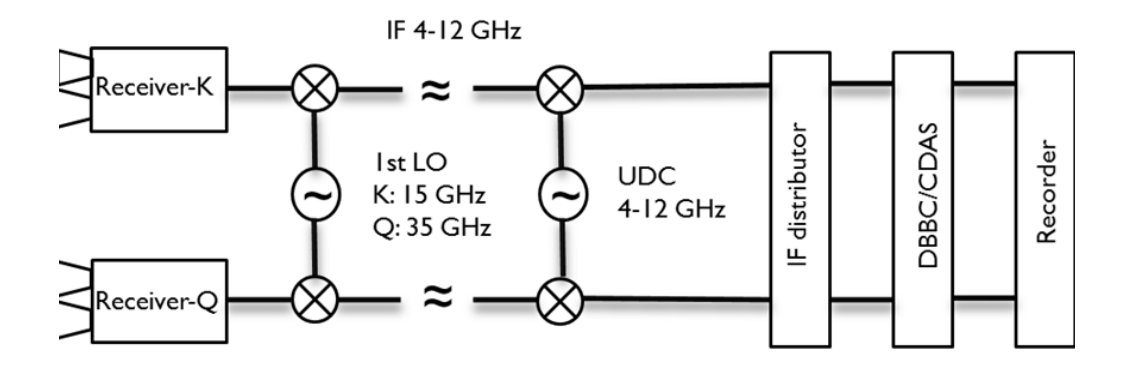


Figure 17: Flow diagram of signals from receiver to recorder for TMRT65.

#### 2.3.8 Brief Summary of SHRT25 Receiving System

The details will be available upon request. Please contact with the EAVN User Support Team if you need further information.

#### 2.3.9 Brief Summary of NSRT26 Receiving System

Figure 18 shows a flow diagram of the VLBI receiving system in NSRT26. NSRT26 has the receivers for 5 frequency bands, L (1.4 GHz), S/X (2.3/8.4 GHz), C (5 GHz), K (22 GHz), and Q (43 GHz), while NSRT26 joins in EAVN observations at only K-band in the 2022A semester. The K-band receiver is cooled HEMT receivers with dual circular polarizers. The observable frequency range and the typical receiver noise temperature are shown in Table 5. The total system noise temperatures at K-band is typically 42 K. The RF signal is down-converted with three stages, and analog-digital conversion and digital filtering of the IF signal is conducted using either the Digital Baseband Converter (DBBC) system or the Chinese VLBI Data Acquisition System (CDAS).

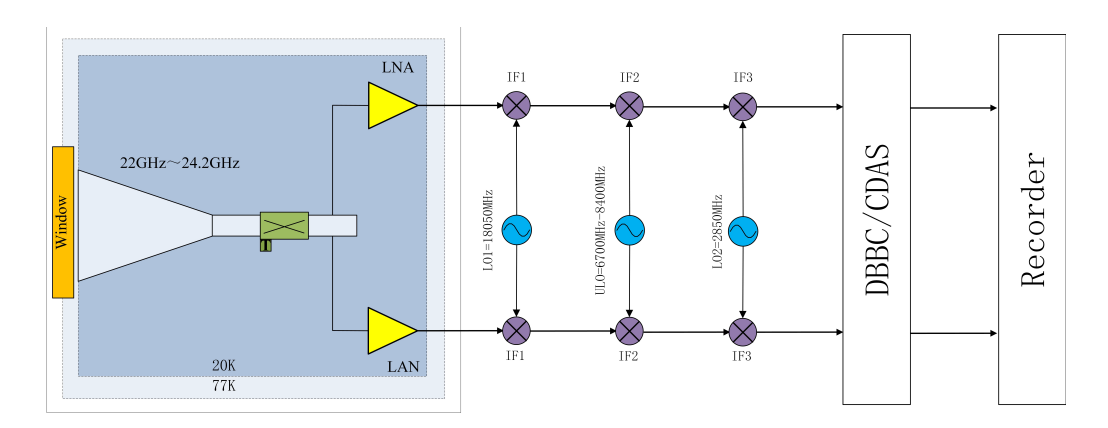


Figure 18: Flow diagram of signals from receiver to recorder for NSRT26.

#### 2.3.10 Brief Summary of KMRT40 Receiving System

Figure 19 shows a flow diagram of the VLBI receiving system in KMRT40. KMRT40 has the receivers for 3 frequency bands, S/X (2.2/8.4 GHz), C (4–8 GHz, Lo is tune-able), while KMRT40 joins in EAVN observations at only C-band in the 2022A semester. The C-band receiver is an HEMT cooled receiver with dual circular polarizations. The observable frequency range and the typical receiver noise temperature are shown in Table 5. The total system noise temperatures at C-band is typically 20 K. The RF signal is down-converted with three stages, and analog-digital conversion and digital filtering of the IF signal is conducted using either the Digital Baseband Converter 2 (DBBC2) system or the Chinese VLBI Data Acquisition System 1 (CDAS1).

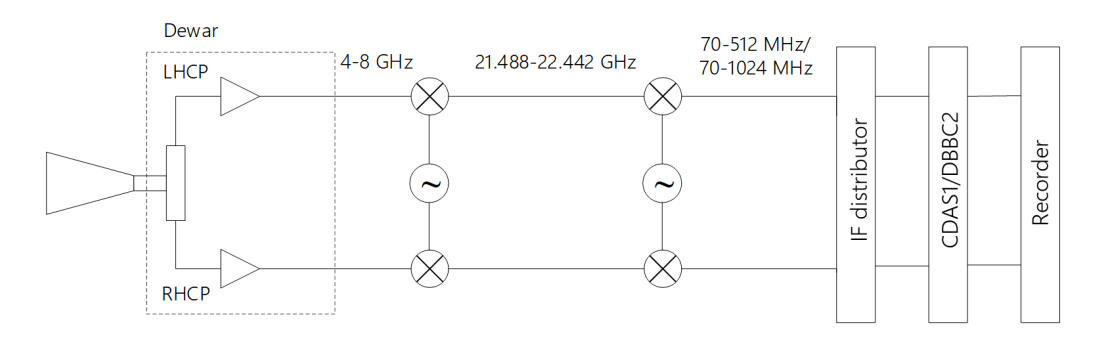


Figure 19: Flow diagram of signals from receiver to recorder for KMRT40.

#### 2.3.11 Brief Summary of KSJ Receiving System

The KSJ antenna has the capability to observe four bands, which are S (2 GHz), X (8 GHz), and simultaneous K/Q (22/43 GHz) bands. Figure 20 shows the layout of quasi-optics and receivers. During the 2022A semester of EAVN observation, K and Q bands are only available. For VLBI performance at 22 and 43 GHz, the KSJ telescope was equipped with the the same LPF used in the KVN telescope, so the receiver noise temperature was significantly improved, indicating  $\sim 31$  K at 22 GHz and  $\sim 86$  K at 43 GHz.

## 2.4 Digital Signal Processing

In VERA system, A/D (analog-digital) samplers convert the analog base band outputs of 0-512 MHz  $\times$  2 beams to digital form. The A/D converters carry out the digitization of 2-bit sampling with the bandwidth of 512 MHz and the data rate is 2048 Mbps for each beam.

In KVN system, A/D samplers digitize signals into 2-bit data streams with four quantization levels. The base band output is 512 – 1024 MHz (1024–1536 MHz in NRO45 Q-band). The sampling rate is 1024 Mega sample per second (Msps) with 2-bit sampling, resulting in the data rate of 2 Gbps at the frequency bandwidth of 512 MHz. Four streams of 512 MHz band width (2 Gbps data rate) can be obtained in the KVN multi-frequency receiving system simultaneously, which means that the total rate is 8 Gbps. In KSJ system, K5 and DBBC3 system are available. The maximum supported data rates of K5 and DBBC3 systems are 1 and 8 Gbps with a

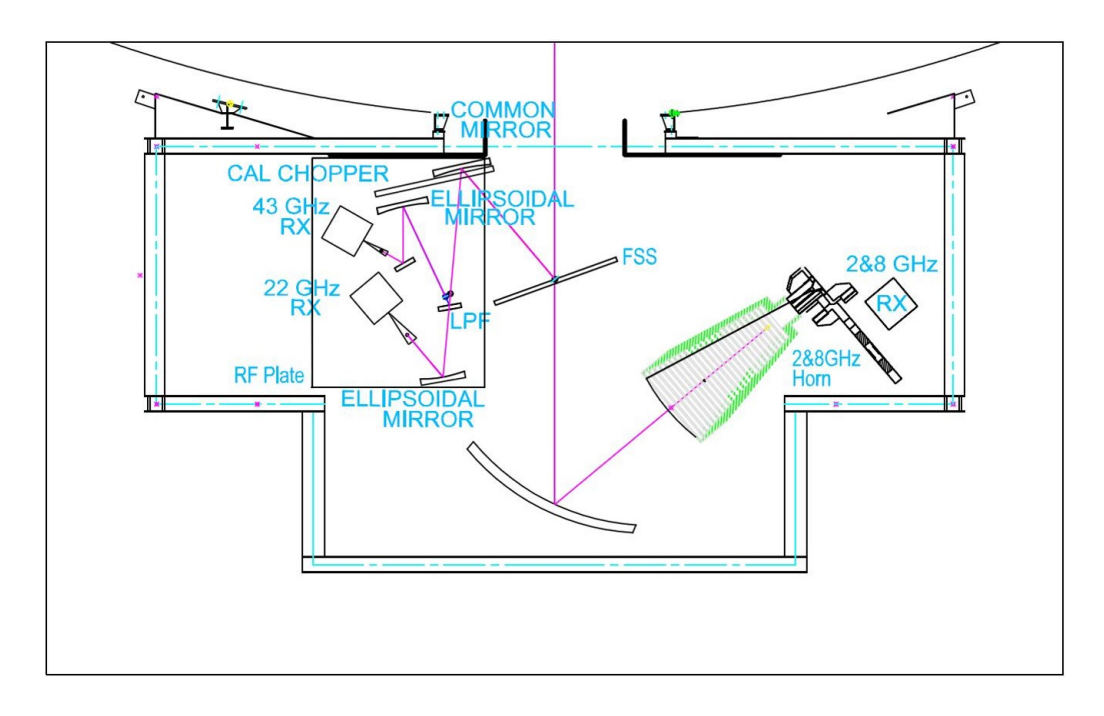


Figure 20: The KSJ quasi-optics and receiving system

2-bit sampling. With K5 and DBBC3 systems, a simultaneous observing mode of S/X and K/Q bands are supported by the KSJ quasi-optics (Figure 20).

In NRO45, TAK32, HIT32, and YAM32 systems, the baseband signal output is 512 – 1024 MHz and the A/D samplers perform 2-bit digitization with four quantization levels. A maximum recording rate of 2048 Mbps is possible with a total bandwidth of 512 MHz.

Since the total data recording rate is limited to 1024 Mbps (see the next section), only part of the sampled data can be recorded onto hard disks. The data rate reduction is done by digital filter system, with which one can flexibly choose number and width of recording frequency bands.

Observers can select modes of the digital filter listed in the Table 6. In VERA7SIOS mode in the Table 6, two transitions (v=1 & 2) of SiO maser in the Q band can be simultaneously recorded.

#### 2.5 Recorders

The EAVN observations are basically limited to record with 1024 Mbps data rate. VERA, NRO45, TAK32, HIT32, and YAM32 have OCTADISK. KVN, TMRT65/SHRT25, NSRT26, and KMRT40 use the Mark5B recording systems. KSJ use the Mark6 recording system. OCTADISK and Mark5B are hard disk recording systems developed at NAOJ and Haystack observatory, respectively. The total bandwidth is 256 MHz.

#### 2.5.1 Note on the Data Storage Capacity

The data for all EAVN observation are recorded using OCTADISK/Mark-5B/Mark-6 data recorder depending on the station. EAVN observation data are usually recorded with the data rate of 1 Gbps, while part of observations (e.g., multi-frequency data

Table 6: Digital filter mode for EAVN.

Mode	Rate	Num.	$BW/CH^b$		Freq. range $^d$	Side	Note for spectral line
Name	(Mbps)	$\mathrm{CH}^a$	(MHz)	$\mathrm{CH}^c$	(MHz)	$\mathrm{Band}^e$	and VERA dual-beam
GEO1K*	1024	16	16	1	0 - 16	U	
				2	32 - 48	U	
				3	64 - 80	U	
				4	96 - 112	U	
				5	128 - 144	U	
				6	160 - 176	U	
				7	192 - 208	U	
				8	224 - 240	U	
				9	256 - 272	U	Target line (e.g. $H_2O$ )
				10	288 - 304	U	
				11	320 - 336	U	
				12	352 - 368	U	
				13	384 - 400	U	
				14	416 - 432	U	
				15	448 - 464	U	
				16	480 - 496	U	
GEO1S*	1024	16	16	1	112 - 128	${ m L}$	
				2	128 - 144	U	
				3	144 - 160	${ m L}$	
				4	160 - 176	U	
				5	176 - 192	${ m L}$	$CH_3OH (J=5_1-6_0 A^+)$
				6	192 - 208	U	
				7	208 - 224	${ m L}$	
				8	224 - 240	U	
				9	240 - 256	${ m L}$	
				10	256 - 272	U	Target line (e.g. $H_2O$ ) <sup><math>j</math></sup>
				11	272 - 288	${ m L}$	
				12	288 - 304	U	
				13	304 - 320	${ m L}$	
				14	320 - 336	U	
				15	336 - 352	${ m L}$	
				16	352 - 368	U	
VERA7SIOS*	1024	16	16	1	32 - 48	U	
				2	64 - 80	U	
				3	80 - 96	${ m L}$	SiO $(J=1-0, v=2)$
				4	96 - 112	U	
				5	128 - 144	U	
				6	160 - 176	U	
				7	192 - 208	U	
				8	224 - 240	U	
				9	256 - 272	U	
				10	288 - 304	U	
				11	384 - 400	U	SiO $(J=1-0, v=1)$
				12	320 - 336	U	, , ,
				13	352 - 368	Ü	
				14	416 - 432	Ü	
				15	448 - 464	Ü	
				16	480 - 496	Ü	
* All channels	and for A I	Doom (Ti	(FDA) and		$\frac{100 \text{ Jgo}}{\text{AVN}}$ . Mode n		tontativo

<sup>\*</sup> All channels are for A-Beam (VERA) and LCP (EAVN). Mode names are tentative.

 $<sup>^</sup>a$  Total number of channels

 $<sup>^</sup>b$ Bandwidth per channel in MHz

<sup>&</sup>lt;sup>c</sup> Channel number

 $<sup>^</sup>d$  Filtered frequency range in the base band (MHz)

<sup>&</sup>lt;sup>e</sup> Side Band (LSB/USB)

 $<sup>^</sup>f$  The total local frequency (i.e., RF frequency corresponding to IF = 0 MHz) is 21,971 MHz for K-band for GEO1K and GEO1S, and 6,488 MHz for C-band for GEO1S.

Table 7: Digital filter mode for EAVN — continued.

Mode	Rate	Num.	$BW/CH^b$	OTT:	Freq. range <sup>d</sup>	Side	Note for spectral line
Name	(Mbps)	$CH^a$	(MHz)	$\mathrm{CH}^c$	(MHz)	$\operatorname{Band}^e$	and VERA dual-beam
VERA4S*	1024	8	32	1	128 - 160	U	
				2	160 - 192	L	
				3	192 - 224	U	
				4	224 - 256	L	
				5	256 - 288	U	
				6	288 - 320	L	
				7	320 - 352	U	
				8	352 - 384	L	
VERA1S*	1024	2	128	1	128 - 256	L	
				2	256 - 384	U	
VERA1**	1024	2	128	1	256 - 384	U	A-Beam
				2	256 - 384	U	B-Beam
VERA7**	1024	16	16	1	256 - 272	U	A-Beam for target line
				2	128 - 144	U	B-Beam (CH 2-16)
				3	144 - 160	${ m L}$	
				4	160 - 176	U	
				5	176 - 192	${ m L}$	
				6	192 - 208	U	
				7	208 - 224	${ m L}$	
				8	224 - 240	U	
				9	240 - 256	${ m L}$	
				10	256 - 272	U	
				11	272 - 288	${ m L}$	
				12	288 - 304	U	
				13	304 - 320	${ m L}$	
				14	320 - 336	U	
				15	336 - 352	${ m L}$	
				16	352 - 368	U	
VERA7MM**	1024	16	16	1	256 - 272	U	A-Beam for target lin
				2	32 - 48	U	B-Beam (CH 2-16)
				3	64 - 80	U	
				4	96 - 112	U	
				5	128 - 144	U	
				6	160 - 176	U	
				7	192 - 208	U	
				8	224 - 240	U	
				9	256 - 272	U	
				10	288 - 304	U	
				11	320 - 336	U	
				12	352 - 368	U	
				13	384 - 400	U	
				14	416 - 432	U	
				15	448 - 464	U	
				16	480 - 496	U	

b Bandwidth per channel in MHz
C Channel number
Filtered frequency range in the base band (MHz)
Side Band (LSB/USB)

recording mode at some of EAVN stations) are conducted using higher data sampling rate of greater than or equal to 2 Gbps. This may give rise to shortage of disk space. If it happens, EAVN operation team may ask PI of each EAVN observation to accept revision of the planned observing schedule.

#### 2.6 Correlators

The correlation process is carried out by a VLBI correlator located at KJCC (Korea-Japan Correlation Center) at Daejeon, which has been developed as the KJJVC (Korea-Japan Joint VLBI Correlator) located at KJCC. Hereafter it is tentatively called "Daejeon correlator". Specification of The Daejeon correlator is summarized in Table 8. The Daejeon correlator can process the data stream of up to 8192 Mbps from maximum 16 antenna stations at once. Currently the raw observed data of KVN, TMRT65/SHRT25, NSRT26, and KMRT40 stations are recorded and playbacked with Mark5B, and those of VERA, NRO45, TAK32, HIT32, and YAM32 are recorded and playbacked with OC-TADISK at the data rate of 1024 Mbps. For KaVA, data formats available in 2022A are 16 IFs × 16 MHz ("C5 mode" in The Daejeon correlator terminology), 8 IFs × 32 MHz (C4 mode), and 2 IFs  $\times$  128 MHz (C2 mode). For EAVN (including non-KaVA telescopes), available data formats are 16 IFs × 16 MHz (C5 mode) at C- and K-band, and 8 IFs  $\times$  32 MHz (C4 mode) at all the C-, K- and Q-bands. Note that the C2 mode is available at only KaVA 7 telescopes because other EAVN telescopes are not equipped with the backend system for the C2 mode. Minimum integration times (time resolution) are 0.2048, 0.8192, and 1.6384 seconds for C2, C4, and C5 modes, respectively, and the number of frequency channels within each IF is 8192 for both modes (i.e. maximum frequency resolution is about 1.95 kHz). By default, the number of frequency channels is reduced to 128 (for continuum) or 512 (for line) via channel integration after correlation. One may put a special request of number of frequency channels to take better frequency resolution. The number of frequency channels can be selected among 512, 1024, 2048, 4096 or 8192. Note that we recommend the maximum frequency channel of 8192 with the C5 mode in the case of CH<sub>3</sub>OH maser observations at C-band to achieve sufficient channel and velocity resolution at IF5 (corresponding to 6,664–6,680 MHz. Final correlated data is served as FITS-IDI file.

#### 2.6.1 Note for the C2 Mode

To obtain the accurate amplitude values across the all IF channels, however, it is better to reduce the number of baseband (or IFs in data handling with AIPS) yielded by the digital filter unit (DFU) so that the amplitude losses at the edge of each baseband are avoided. This reduction is especially helpful to observe continuum sources, such as active galactic nuclei (AGN). For this purpose, C2 mode, which has 2 IFs  $\times$  128 MHz, is opened for EAVN although the mode can be employed for an observation with only KaVA 7 telescopes.

When using the C2 mode, note the following two matters: (i) There is a moderate amplitude slope in an IF channel mainly at VERA stations, which must be corrected by all the gain calibration procedures in AIPS (AIPS tasks ACCOR, BPASS, and APCAL): (ii) KaVA's observation data is conventionally correlated by the Daejeon Hardware Correlator. In this case, the scaling factor of 1.3 should be applied to the

data to recover the quantization loss <sup>1</sup> [12].

Table 8: Specification of The Daejeon correlator<sup>a</sup>.

Table 6. Specific	ation of the Daejeon Correlator.
Max. number of antennas	16
correlation mode	$C2^b$ (128 MHz Bandwidth, 2 stream)
	C4 (32 MHz Bandwidth, 8 stream)
	C5 (16 MHz Bandwidth, 16 stream)
Max. number of corr./input	120  cross + 16  auto
Sub-array	2 case (12+4, 8+8)
Bandwidth	$512~\mathrm{MHz}$
Max. data rate/antenna	2048 Mbps VSI-H (32 parallels, 64 MHz clock)
Max. delay compensation	$\pm$ 36,000 km
Max. fringe tracking	$1.075~\mathrm{kHz}$
FFT work length	16+16 bits fixed point for real, imaginary
Integration time	$25.6~\mathrm{msec} \sim 10.24~\mathrm{sec}$
Data output channels	8192 channels
Data output rate	Max. 1.4 GB/sec at 25.6 msec integration time
aT 1 . 11 . 1 0 11	

<sup>&</sup>lt;sup>a</sup>For more details, see the following website: https://radio.kasi.re.kr/kjcc/main\_kjcc.php <sup>b</sup>This mode is available for only KaVA.

#### 2.7 Calibration

Here we briefly summarize the calibration procedure of the EAVN data. Basically, most of the post-processing calibrations are done by using the AIPS (Astronomical Image Processing System) software package developed by NRAO (National Radio Astronomical Observatory).

#### 2.7.1 Delay and Bandpass Calibration

The time synchronization for each antenna is kept within 0.1  $\mu$ sec using GPS and high stability frequency standard provided by the hydrogen maser. To correct for clock parameter offsets with better accuracy, bright continuum sources with accurately-known positions should be observed at usually every 60-80 minutes during observations. A recommended scan length for calibrators is 5-10 minutes. This can be done by the AIPS task FRING. The calibration of frequency characteristic (bandpass calibration) can be also done based on the observation of bright continuum source. This can be done by the AIPS task BPASS.

#### 2.7.2 Gain Calibration

VERA, KVN, NRO45, TAK32, and HIT32 antennas have the chopper wheel of the hot load (black body at the room temperature), and the system noise temperature can be obtained by measuring the ratio of the sky power to the hot load power (so-called R-Sky method). Thus, the measured system noise temperature is a sum of the receiver noise temperature, spillover temperature, and contribution of the atmosphere (i.e. so-called  $T_{\text{sys}}^*$  corrected for atmospheric opacity). The hot load measurement can be made

<sup>&</sup>lt;sup>1</sup>This scaling factor is conventionally applied to the data using the AIPS task APCAL, however this is not applicable if the data is loaded to AIPS using the AIPS task FITLD with DIGICOR = 3.

before/after any scan at all telescopes except TAK32 and HIT32. TAK32 and HIT32 measure the hot-load power at the timing when the telescope operator decides to do the measurement before or after any scan. The sky power is continuously monitored during scans, so that one can trace the variation of the system noise temperature. The system noise temperature value can be converted to SEFD (System Equivalent Flux Density) by dividing by the antenna gain in K/Jy, which is derived from the aperture efficiency and diameter of each antenna. For the correlated data from KJCC,  $T_{\rm sys}^*$  data (TY table) and antenna gain information (GC table) are provided with the ANTAB-readable format. KJCC makes complete version of ANTAB-readable file and provide it to PI. User support team supports PIs as appropriate. The TY and GC tables can be loaded by the AIPS task ANTAB, and these tables are converted to the SN table by the AIPS task APCAL.

On the other hand,  $T_{\text{sys}}$  measurement provided by TMRT65, SHRT25, and NSRT26 contains atmospheric opacity effects, thus the opacity correction should be applied to those data in the course of data reduction.

Alternatively, one can calibrate the visibility amplitude by the template spectrum method, in which auto-correlation spectra of a maser source is used as the flux calibrator. This calibration procedure is made by the AIPS task ACFIT (see AIPS HELP for ACFIT and [3] for more details). For an EAVN observation including TMRT65, NRO45, TAK32, HIT32, NSRT26, and SHRT25, we strongly recommend users to observe a maser source or a compact continuum gain calibrator for every  $\leq 1$  hr. This offers an additional cross-check of the amplitude calibration for TMRT65 and NRO45. YAM32 antenna is not equipped with any system noise temperature measurement system, and hence, it is mandatory to observe a maser source for the gain calibration and absolute flux scaling via the template spectrum method. KMRT40 antenna has a problem with the control program on the system of injecting noise source at each scan during observations, and hence, it is mandatory to observe a maser source for achieving the template spectrum method as well like the situation of YAM32. In particular during elevations lower than 20°, it is recommended to observe these calibrators every 30 min or shorter. Please see Section 3.11 for more details. The DPFU values used in the AIPS task ACFIT are listed in Table 4.

Further correction is made for VLBI observations taken with 2-bit (4-level) sampling, for the systematic effects of non-optimal setting of the quantizer voltage thresholds. This is done by the AIPS task ACCOR. Another correction should be applied to recover the amplitude loss, which are attributed to the combination of two steps of 2-bit quantization in the digital filtering at the backend system and characteristics of Daejeon correlator. This is done by multiplying the scaling factor of 1.3 (the best current estimation) [12] in the AIPS task APCAL (adverbs APARM(1) = 1.3, OPCODE = ", and DOFIT = 1) or SNCOR (adverbs OPCODE = "MULA", and SNCORPRM(1) = 1.3). Note that this correction should be applied to all EAVN telescopes. The amplitude calibrations with EAVN are accurate to 15% or better at both K- and Q-bands.

For HIT32 at C-band, we recommend to flag the specified frequencies at the beginning of the data reduction: RF 6,600–6,648 due to the IF filtering for anti-alias, and RF 6,712–6,760 MHz due to the Notch-filtering for flagging strong spurious. For example, after the digital filtering with GEO1S mode for HIT32 data, these frequencies correspond to IFs 1–3 and 8–10

in the correlated data in the C5 correlation mode (16 MHz  $\times$  16 IFs). This flagging process is done by the AIPS task UVFLG.

#### 2.7.3 Pointing Correction

The EAVN two large telescopes, TMRT65 and NRO45, will carry out regular antenna pointing scans for every  $\leq 1-2$  hr. As for TMRT65, moreover, frequent pointing check is necessary for observations at both K- and Q-bands. The pointing check is done semi-automatically with a continuum back-end system and the quality of pointing check is judged by on-site operators. We strongly recommend to keep at least 3 minutes for the pointing check itself with additional slewing time between target and pointing sources. For example, it is preferable to secure 5-min gap in total for the pointing check toward a pointing source with the angular separation of  $\sim 15^{\circ}$  from the target.

#### 2.8 Geodetic Measurement

#### 2.8.1 Brief Summary of VERA Geodetic Measurement

Geodetic observations are performed as part of the VERA project observations to derive accurate antenna coordinates. The geodetic VLBI observations for VERA are carried out in the S/X-bands and also in the K-band. The S/X-bands are used in the domestic experiments with the Geographical Survey Institute of Japan and the international experiments called IVS-T2. On the other hand, the K-band is used in the VERA internal experiments. We obtain higher accuracy results in the K-band compared with the S/X-bands. The most up-to-date geodetic parameters are derived through geodetic analyses.

Non-linear post seismic movement of Mizusawa after the 2011 off the Pacific coast of Tohoku Earthquake continues. The position and velocity of Mizusawa is continuously monitored by GPS. The coordinates in Table 1 are provisional and will be revised with accumulation of geodetic data by GPS and VLBI.

In order to maintain the antenna position accuracy, the VERA project has three kinds of geodetic observations. The first is participation in JADE (JApanese Dynamic Earth observation by VLBI) organized by GSI (Geographical Survey Institute) and IVS-T2 session in order to link the VERA coordinates to the ITRF2008 (International Terrestrial Reference Frame 2008). Basically Mizusawa station participates in JADE nearly every month. Based on the observations for four years, the three-dimensional positions and velocities of Mizusawa station till 2011 March 9 is determined with accuracies of 7-9 mm and about 1 mm/yr in ITRF2008 coordinate system. But the uncertainty of several centimeters exists in the position on and after 2011 March 11. The second kind of geodetic observations is monitoring of baseline vectors between VERA stations by internal geodetic VLBI observations. Geodetic positions of VERA antennas relative to Mizusawa antenna are measured from geodetic VLBI observations every two weeks. From polygonal fitting of the six-year geodetic results, the relative positions and velocities are obtained at the precisions of 1-2 mm and 0.8-1 mm/yr till 2011 March 10. The third kind is continuous GPS observations at the VERA sites for interpolating VLBI geodetic positions. Daily positions can be determined from 24 hour GPS data. The GPS observations are also used to estimate tropospheric zenith delay of each VERA site routinely. The time resolution of delay estimates is 5 minutes.

#### 2.8.2 Brief Summary of KVN Geodetic Measurement

KVN has been participating K band geodetic VLBI observations with VERA on behalf of KaVA geodesy program since 2011. In addition, the invariant point (IVP) coordinates of the KVN Ulsan and Tamna telescopes has been measured from the optical survey using GNSS and optical instruments. Please refer [20]. for more details. At present, the formal errors of KVN IVP in geodetic VLBI is around 3-5 mm and the difference between VLBI and GNSS is about 2 cm level.

## 3 Observing Proposal

### 3.1 Call for Proposals (CfP)

We invite proposals for the open-use observations of EAVN. Please refer to the following EAVN webpage for more details about the array and its performance, and how to prepare and submit a proposal.

#### http://eavn.kasi.re.kr/

This EAVN open-use call provides opportunities of VLBI observations at 6.7 GHz (C-band), 22 GHz (K-band), and 43 GHz (Q-band) for astronomers in the world. If proposers are not familiar with EAVN, they are recommended to include at least one collaborator from EAVN. The contact address for the support is eavnhelp(at mark)kasi.re.kr.

EAVN observations are conducted with single polarization (LHCP<sup>2</sup>) and the data are recorded with the data rate of 1 Gbps. The data obtained at NRO45, TAK32, HIT32, and YAM32 are recorded with the data rate of 2 Gbps and reformatted to 1 Gbps data at Mizusawa VLBI Observatory of NAOJ. The total observation time for EAVN is up to 500 hours, while the available observing time for each EAVN telescope is different between each other, as shown in Table 9.

Special conditions to be considered for EAVN proposal submission are shown below.

#### 3.1.1 Total telescope time and maximum of total request time (see Table 9)

- Total telescope time for KaVA is 500 hours. Proposers can request for the KaVA's telescope time (VERA+KVN) without limitation from 2021B (c.f. up to 100 hours for one proposal until 2021A), while the maximum total request time per one proposal is 50 hours (36, 24 hours for some telescopes) for EAVN (inclusion of non-KaVA telescopes). Note that a proposal for the Large Program will not be accepted for the 2022A semester. Note also that KaVA is a mandatory array for all EAVN observations.
- Total telescope time for NRO45 is 50 hours, and proposers can request for the maximum total observation time of 24 hours for one proposal. Please include 1-hour additional time for overhead to each observing epoch in NRO45's total request time if your proposal requires NRO45 to join. If your proposal consists of two-epoch observations with the observing time of 8 hours per epoch with NRO45, for example, total request time for NRO45 shall be 18 hours (= (8 + 1) hours × 2 epochs).
- Sum of total telescope time for TMRT65 and SHRT25 is 150 hours. Proposers can request for the telescope time of up to 50 hours for TMRT65/SHRT25 for one proposal. Note that proposers cannot request for inclusion of both TMRT65 and SHRT25 in your project. SHRT25 will join in EAVN C-band observations in substitution of TMRT65 in case TMRT65 cannot conduct EAVN observations.
- Total telescope time for NSRT26 is 150 hours. **Proposers can request for the** telescope time of up to 50 hours for NSRT26 for one proposal.

<sup>&</sup>lt;sup>2</sup>RHCP is used for the simultaneous K/Q band mode (see Section 4.4).

Table 9.	Available	observing	time a	and frea	nency for	each	EAVN	telescope.
Table 5.	TIVALIANIC	ODDOL VIIIS	UIIIIC O	mid ii cq	uciic y ioi	Cacii	T11111	ocioscopo.

Max. request							
Array/	Total	time for one	Frequency				
Telescope	time [h]	proposal [h]	C-band	K-band	Q-band		
KaVA	500		$ullet^1$	•	•		
Tianma (TMRT65)/	$150^{2}$	50	•	•	•		
Sheshan (SHRT25)	_		•				
Nanshan (NSRT26)	150	50		•			
Kunming (KMRT40)	$50^{3}$	$36^{3}$	•				
Nobeyama (NRO45)	36	24		•	•		
Takahagi (TAK32)	50	36		•			
Hitachi (HIT32)	50	36	$ullet^4$				
Yamaguchi (YAM32)	50	36	$ullet^4$				
Sejong (KSJ)	$100^{5}$	24		•	•		

- 1: Five telescopes (VERA's 4 telescopes and KVN Ulsan) out of KaVA's 7 telescopes join in EAVN observations at C-band.
- 2: Available time of the TMRT65 and SHRT25 antennas is 150h in total (not 150h for each).
- 3: Exactly total time and maximum time for one proposal is depends on its national missions, but negotiable.
- 4: HIT32 and YAM32 are simultaneously involved in EAVN open-use observations at C-band. Proposers shall not be able to choose only one of either HIT32 or YAM32 for their EAVN observations.
- 5: Sejong's telescope time is shared between EAVN open-use program (this call) and KVN open-use program.
- Total telescope time for KMRT40 is 50 hours, and proposers can request for the telescope time of up to 36 hours for one proposal. KMRT40 does not guarantee proposers to completely use its time, due to any sudden national missions. So the exact total time and maximum time for one proposal must depends on its national missions, but it is negotiable.
- Total telescope time for TAK32, HIT32, and YAM32 is 50 hours each. Proposers can request for the telescope time of up to 36 hours for each TAK32, HIT32, and YAM32 for one proposal.

YAM32 has a problem with the hydrogen maser (H-maser) and does not conduct a VLBI observation since the 2021B semester. They plan to introduce an oven controlled crystal oscillator (OCXO) and to check its stability by the end of 2021 (results of the stability check will be informed via the EAVN website once OCXO is installed. An integration time, however, will be limited to less than 100 sec at 6.7 GHz due to less stability of OCXO compared to that of an H-maser, resulting in difficulty in detecting a weak source.

Please take into account the situation in Yamaguchi shown above if you plan to request usage of YAM32 in your proposal, and note that YAM32 shall not participate in EAVN observations in the 2022A semester depending on the status of the frequency standard.

• Total telescope time for KSJ is 100 hours and proposers can request for the

telescope time of up to 24 hours for one proposal, while this telescope time is shared between EAVN open-use program (this call) and KVN open-use program. How to share KSJ's telescope time will be discussed between the Time Allocation Committee of EAVN and KVN on the basis of proposal review results. Note also that KSJ participates in EAVN open-use program in the 2022A semester with shared-risk mode for all observing modes to be provided.

#### 3.1.2 Term of EAVN observation

- All EAVN observations will be scheduled between 2022 January 16 and 2022 June 15, while possible term of observation for each array/telescope is different between each other, as mentioned below.
- NRO45's telescope time will be allocated to two or three days during 2022 March 21 and March 31, while the detailed schedule will be negotiated later. EAVN observations including NRO45 can be assigned to the same LST range up to 3 times in two adjacent semesters (2021B and 2022A). In the 2022A semester, approval of a proposal including NRO45 for the following LST range shall be limited.
  - LST 07:30 17:30: To be approved for up to two epochs.
  - LST 18:30 22:30: To be approved for up to two epochs.

#### 3.1.3 Possible array configuration

- KaVA is a mandatory array for all EAVN observations.
- At K- and Q-bands, EAVN accepts a request for usage of sub-array configuration (KaVA 7 telescopes and additional telescopes from NRO45, TMRT65, NSRT26, TAK32, and KSJ for K-band and KaVA 7 telescopes and additional telescopes from NRO45, TMRT65, and KSJ for Q-band) as well as EAVN full array configuration with 12 or 10 telescopes at K- or Q-band, respectively. A proposer shall clarify the reason for the choice of sub-array configuration in the proposal.
- HIT32 and YAM32 shall be simultaneously involved in EAVN open-use observations at C-band. Proposers shall not be able to choose only one of either HIT32 or YAM32 for their EAVN observations. Table 10 summarizes possible array configuration for EAVN observations at C-band.
- At C-band, either TMRT65 or SHRT25 will join the EAVN observations. When TMRT65 is not available, SHRT25 will be used in the EAVN observations.

In summary, non-KaVA telescopes (TMRT65/SHRT25, NSRT26, KMRT40, NRO45, TAK32, HIT32, YAM32, and KSJ) will participate in EAVN observations together with KaVA according to scientific needs and their availability. Note that proposals submitted to EAVN can be assigned to KaVA according to the decision by the EAVN Time Allocation Committee (TAC).

EAVN proposal submission deadline is at

Table 10: Possible array configuration at C-band.

Configuration	Telescope							
	KaVA <sup>a</sup>	$TMRT65/SHRT25^b$	KMRT40	$HIT32^c$	$YAM32^c$			
1	•	0						
2	•	0	•					
3	•	0		•	•			
4	•		•					
5	•			•	•			
6	•		•	•	•			
7	•	0	•	•	•			

<sup>&</sup>lt;sup>a</sup> KaVA includes VERA 4 telescopes and KVN Ulsan (i.e. total 5 telescopes).

#### 08:00 UT on 1 November, 2021.

Detailed information on the EAVN call-for-proposal can be found in the following webpage:

https://radio.kasi.re.kr/eavn/proposal info.php

### 3.2 Proposal Submission

The EAVN proposal application form and proposal submission are available at the EAVN website. If you have any questions regarding to your proposal submission, contact to "eavnprop(at mark)kasi.re.kr". A proposal shall contain the coversheet (two pages), scientific and technical justification including figures and tables (maximum of three pages) with the minimum font size of 10 points. The results of the review will be announced to each PI by early January, 2022.

## 3.3 Special Condition for Selecting Proposals

All submitted proposals for EAVN are reviewed by referees and the EAVN TAC allocates the observing time based on the referee's rating. A proposal submitted for EAVN observations could be allocated as KaVA observations depending on its rating and the decision made by TAC. Proposers thus should specify the necessity of including non-KaVA telescopes in your observations.

## 3.4 Policy of Recovery Observations

If an open use observation has more than one missing station due to system trouble and/or very severe weather conditions (e.g. strong wind due to a typhoon), the PI can request recovery observations within a year of receiving the correlated data. The EAVN TAC will consider the time allocation of the recovery observations for the next season. This policy is applied to EAVN telescopes except NRO45, KMRT40, and KSJ i.e., KVN, VERA, TMRT65/SHRT25, NSRT26, TAK32, HIT32 and YAM32.

<sup>&</sup>lt;sup>b</sup> Either TMRT65 or SHRT25 will join in EAVN observations.

<sup>&</sup>lt;sup>c</sup> HIT32 and YAM32 shall be simultaneously involved in EAVN observations.

## 3.5 Policy of One-year-long Proposals

EAVN abolishes accepting a proposal requesting one-year-long observations from the 2021B semester<sup>3</sup>. One should thus submit a proposals by a submission deadline for each semester.

#### 3.6 Observation Mode

EAVN provides opportunities of observations at three observing frequencies, 6.7 GHz (C-band), 22 GHz (K-band), and 43 GHz (Q-band). All EAVN observations are conducted with single polarization (LHCP<sup>4</sup>) and with the data recording rate of 1 Gbps (total bandwidth of 256 MHz). Three types of setup of the digital filter ('C2 mode' with 2 IFs × 128 MHz, 'C4 mode' with 8 IFs × 32 MHz, and 'C5 mode' with 16 IFs × 16 MHz) are available, while the C2 mode is not available if your proposal contains requests for usage of non-KaVA stations. The C4 mode is available at all the frequencies, while the C5 mode can be used at both C- and K-bands. EAVN accepts a proposal using the 'Multi-frequency data recording mode' in which KVN records the observation data at more than one frequency, while total number of sessions using this mode might be limited depending on capability of disk storage.

Available observing mode of EAVN is summarized in Tables 11 and 12.

Table 11: Available observing mode of EAVN.

Frequency	C-band	K-band	Q-band
Telescope	VERA, KVN-Ulsan,	KaVA, KSJ,	KaVA, KSJ,
	TMRT65/SHRT25,	NRO45, TMRT65,	NRO45, TMRT65
	KMRT40,	NSRT26, TAK32	(10 telescopes)
	HIT32, YAM32	(12 telescopes)	
	(9 telescopes)		
Backend mode	$C4, C5^a$	$C2^{b}, C4, C5$	$C2^b$ , $C4$ , $C5^c$
Recording rate		$1 \text{ Gbps}^d$	
Polarization	Left-hand	circular polarization (I	$LHCP)^e$
Correlator	Dae	jeon Hardware Correlat	or

<sup>&</sup>lt;sup>a</sup> For maser observations, C5 mode is strongly recommended to achieve sufficiently high channel resolution.

# 3.7 Possible Conflict/duplication with Large Programs

In order to avoid conflict and/or duplication of the targets with existing KaVA Large Programs (LPs), proposers are highly recommended to visit the KaVA LP webpage

 $<sup>^</sup>b$  C2 mode is available at only KaVA telescopes.

 $<sup>^{</sup>c}$  C5 mode is available at KaVA and TMRT65.

 $<sup>^</sup>d$  Data obtained at NRO45, TAK32, HIT32, and YAM32 are recorded with 2 Gbps and reprocessed to 1 Gbps.

 $<sup>^</sup>e$  RHCP is used for the simultaneous K/Q band mode (see Section 4.4).

 $<sup>^3{\</sup>rm EAVN}$  had been accepting a proposal requesting for the observing term of two consecutive semesters until the 2021A semester.

<sup>&</sup>lt;sup>4</sup>RHCP is used for the simultaneous K/Q band mode (see Section 4.4).

Table 12: Available observing mode for each EAVN telescope.

									1		
Telescope	I	Band	l		Observing mode						
	С	K	Q	$T.I.^a$	F.S. <sup>b</sup>	$\mathrm{HB}^c$	$\mathrm{WFI}^d$	$K/Q^e$	$\mathrm{ToO}^f$		
KaVA	$ullet^g$	•	•	•	•	•	•	•	•		
TMRT65	•	•	•	•					•		
NSRT26		•		•	•				•		
KMRT40	•			•	•						
NRO45		•	•	•				•			
TAK32		•		•					•		
HIT32	•			•	•				•		
YAM32	•			•	•				•		
SHRT25	•			•	•				•		
KSJ		•	•	•	•			•			

<sup>&</sup>lt;sup>a</sup> Total intensity imaging.

where KaVA LPs and their source lists are presented:

https://radio.kasi.re.kr/kava/large programs.php.

Proposals to be submitted for this opportunity should not have the same scientific goal with LPs, while it is fine to propose same sources with LPs if your proposal has a different scientific goal with LPs.

# 3.8 Target of Opportunity (ToO) Observations

EAVN accepts ToO proposals. Proposers can request the participation of **TMRT65**/SHRT25, NSRT26, HIT32, TAK32, and YAM32 as well as KaVA for ToO observations, while these non-KaVA telescopes will join only on a best effort basis. Note that NRO45, KMRT40, and KSJ cannot be included for ToO proposals. **Total approved time for ToO proposals is limited to be 100 hours in the 2022A semester.** 

It is strongly recommended that ToO proposals (especially expected ToO) are submitted during the regular CfP. Unexpected or urgent ToO can be submitted as Director's Discretionary Time (DDT) proposals. ToO proposals must include clear triggering criteria to initiate an observation. ToOs are valid for one year after it is approved. ToO proposals for DDT should follow the same format of regular call and should be sent to "eavnprop(at mark)kasi.re.kr".

<sup>&</sup>lt;sup>b</sup> Fast antenna switching. See Section 4.1.

<sup>&</sup>lt;sup>c</sup> 1-beam hybrid mode. See Section 4.2.

<sup>&</sup>lt;sup>d</sup> Wide-field imaging with short accumulation period. See Section 4.3.

 $<sup>^</sup>e$  K/Q-band simultaneous observation mode. See Section 4.4.

<sup>&</sup>lt;sup>f</sup> Target of opportunity. See Section 3.8.

 $<sup>^{</sup>g}$  VERA four stations and KVN Ulsan station.

## 3.9 Angular Resolution and Largest Detectable Angular Scale

The maximum angular resolution for EAVN observations is 2.4 mas at C-band for VERA-Ogasawara – KMRT40 baseline, 0.55 mas at K-band for VERA-Ogasawara – NSRT26 baseline, and 0.63 mas at Q-band for VERA-Mizusawa – VERA-Ishigakijima baseline in 2022A. The synthesized beam size strongly depends on UV coverage, and could be larger than the values mentioned above because the baselines projected on UV plane become shorter than the distance between telescopes. The beam size can be calculated approximately by the following formula;

$$\theta \sim 2063 \left(\frac{\lambda}{[\text{cm}]}\right) \left(\frac{B}{[\text{km}]}\right)^{-1} [\text{mas}],$$
 (2)

where  $\lambda$  and B are observed wavelength in centimeter and the maximum baseline length in kilometer, respectively.

The minimum detectable angular scale for interferometers can be also expressed by equation (2), where the baseline length B is replaced with the shortest one among the array. Because of the relatively short baselines provided by KVN,  $\sim 300$  km, KaVA is able to detect an extended structure up to 9 mas and 5 mas for the K- and Q-bands, respectively. In the case of C-band, the first, second, and third shortest baseline formed by KVN-Ulsan – YAM32, VERA-Mizusawa – HIT32 and VERA-Iriki – YAM32 is similar to be  $\sim 260$  km,  $\sim 270$  km and  $\sim 290$  km, yielding 36, 34 and 32 mas in C-band, respectively. The above (red-colored) sentense describes EAVN perfomance, thus, this sentense should be moved to the following paragraph.

As for an EAVN array in which non-KaVA stations (except NSRT26 and KMRT40) are added to KaVA, the longest/shortest baselines remain the same as those of KaVA. The shortest baseline is  $120\,\mathrm{km}$  between KYS and KSJ. The maximum angular resolutions and the largest detectable angular scales are thus basically the same, although their detailed values in a synthesized image are dependent on the scheme of UV weighting as well as the UV coverage. As for an EAVN array which additionally includes KMRT40 and NSRT26 at C-band and K-band, the longest baseline length extends to  $3874\,\mathrm{km}$  and  $5100\,\mathrm{km}$  (primarily along the east-west direction), respectively. This enhances the maximum angular resolution at C-band and K-band of EAVN from 2021B by a factor of  $\sim 2$  and  $\sim 3$  compared to that of KaVA, respectively.

As for an EAVN array in which non-KaVA stations (except NSRT26 and KMRT40) are added to KaVA, the shortest baseline became 120 km between KYS and KSJ. Thus the largest detectable angular scales will be improved by a factor of  $\sim 2.5$  in K- and Q-band. In the case of C-band where KSJ does not participate, the first, second, and third shortest baseline formed by KVN-Ulsan – YAM32, VERA-Mizusawa – HIT32 and VERA-Iriki – YAM32 is similar to be  $\sim 260$  km,  $\sim 270$  km and  $\sim 290$  km, yielding 36, 34 and 32 mas in C-band, respectively. Because the longest baselines remain unchanged, the maximum angular resolutions are basically the same as those of KaVA, although their detailed values in a synthesized image are dependent on the scheme of UV weighting as well as the UV coverage. As for an EAVN array which additionally includes KMRT40 and NSRT26 at C-band and K-band, the longest baseline length extends to 3874 km and 5100 km (primarily along the east-west direction), respectively. This enhances the maximum angular resolution at C-band and K-band of EAVN from 2021B by a factor of  $\sim 2$  and  $\sim 3$  compared to that of KaVA, respectively.

## 3.10 Sensitivity

When a target source is observed, a noise level  $\sigma_{\rm bl}$  for each baseline can be expressed as

$$\sigma_{\rm bl} = \frac{2k}{\eta} \frac{\sqrt{T_{\rm sys,1} T_{\rm sys,2}}}{\sqrt{A_{e,1} A_{e,2}} \sqrt{2B\tau}} = \frac{1}{\eta} \frac{\sqrt{SEFD_1 SEFD_2}}{\sqrt{2B\tau}},\tag{3}$$

where k is Boltzmann constant,  $\eta$  is quantization efficiency ( $\sim 0.88$ ),  $T_{\rm sys}$  is system noise temperature, SEFD is system equivalent flux density,  $A_e$  is antenna effective aperture area ( $A_e = \pi \eta_A D^2/4$  in which  $\eta_A$  and D are the aperture efficiency and antenna diameter, respectively), B is the bandwidth, and  $\tau$  is on-source integration time. Note that for an integration time beyond 3 minutes (in the K-band), the noise level expected by equation (3) cannot be attained because of the coherence loss due to the atmospheric fluctuation. Thus, for finding fringe within a coherence time, the integration time  $\tau$  cannot be longer than 3 minutes. For VLBI observations, signal-to-noise ratio (S/N) of at least 5 and usually 7 is generally required for finding fringes.

A resultant image noise level  $\sigma_{\rm im}$  can be expressed as

$$\sigma_{\rm im} = \frac{1}{\sqrt{\Sigma \sigma_{\rm bl}^{-2}}}. (4)$$

If the array consists of identical antennas, an image noise levels can be expressed as

$$\sigma_{\rm im} = \frac{2k}{\eta} \frac{T_{\rm sys}}{A_e \sqrt{N(N-1)B\tau}} = \frac{1}{\eta} \frac{SEFD}{\sqrt{N(N-1)B\tau}},\tag{5}$$

where N is the number of antennas. Using the typical parameters shown in Tables 13-15, baseline and image sensitivity values of EAVN can be calculated as listed in Tables 13-15 and Table 16, respectively (baseline and image sensitivities of KVN, VERA, and KaVA, as well as EAVN, are also shown for reference). Tables 13-15 contains all combinations of baselines, while Table 16 indicates part of possible combinations of telescopes.

	Ante	nna per	rformance		Baseline sensitivity							
	$T_{\rm sys}$ $\eta_{\rm A}$ SEFI		SEFD	VERA	TMRT65	SHRT25	KMRT40	HIT32	YAM32			
	[K]		[Jy]									
KVN Ulsan	330	0.62	4241	13.9	2.2	12.5	5.2	3.8	5.0			
VERA	130	0.53	2155	9.9	1.6	8.9	3.7	2.7	3.6			
TMRT65	30	0.45	55	_	_	_	0.6	0.4	0.6			
SHRT25	130	0.42	1740	_	_	_	3.4	2.4	3.2			
KMRT40	35	0.25	307	_	_	_	_	1.0	1.4			
HIT32	30	0.65	158	_	_	_	_	_	1.0			
YAM32	50	0.60	286	_	_	_	_	_	_			

Table 13: Performance of EAVN at C-band.

Note: The  $1\sigma$  baseline sensitivity values are listed in unit of mJy, which assume an integration time of 120 seconds and a bandwidth of 256 MHz for the calculation. In the case of narrower bandwidth of 1.953 kHz (for maser emission), sensitivities can be calculated by multiplying a factor of 362.

Table 14: Performance of EAVN at K-band.

	Ante	nna pei	rformance		Baseline sensitivity							
	$T_{\rm sys}$	$\eta_{ m A}$	SEFD	KVN	VERA	TMRT65	NRO45	NSRT26	TAK32	KSJ		
	[K]		[Jy]									
KVN	100	0.6	1328	6.1	7.7	1.7	2.8	3.2	3.1	5.9		
VERA	120	0.5	2110	_	9.7	2.1	3.6	4.0	3.9	7.4		
TMRT65	60	0.5	100	_	_	_	0.8	0.9	0.8	1.6		
NRO45	100	0.61	285	_	_	_	_	1.5	1.4	2.7		
NSRT26	42	0.6	364	_	_	_	_	_	1.6	3.1		
TAK32	40	0.3	343	_	_	_	_	_	_	3.0		
KSJ	100	0.59	1231	_	_	_	_	_	_	_		

Note: The  $1\sigma$  baseline sensitivity values are listed in unit of mJy, which assume an integration time of 120 seconds and a bandwidth of 256 MHz for the calculation. In the case of narrower bandwidth of 15.625 kHz (for maser emission), sensitivities can be calculated by multiplying a factor of 128.

Table 15: Performance of EAVN at Q-band.

	Ante	nna per	formance		Baseline sensitivity						
	$T_{\rm sys}$ $\eta_{\rm A}$ SEFD		KVN	VERA	TMRT65	NRO45	KSJ				
	[K]		[Jy]								
KVN	150	0.6	1992	9.1	13.6	2.3	5.2	9.3			
VERA	250	0.5	4393	_	20.1	3.4	7.8	13.8			
TMRT65	66	0.45	122	_	_	_	1.3	2.3			
NRO45	200	0.53	655	_	_	_	_	5.3			
KSJ	150	0.53	2055	_	_	_	_				

Note: The  $1\sigma$  baseline sensitivity values are listed in unit of mJy, which assume an integration time of 120 seconds and a bandwidth of 256 MHz for the calculation. In the case of narrower bandwidth of 15.625 kHz (for maser emission), sensitivities can be calculated by multiplying a factor of 128.

Figures 21 and 22 show the system noise temperature at VERA and KVN-Ulsan in K/Q-bands, and VERA-Ogasawara in C-band, respectively. VERA, receiver noise temperatures are also plotted.

Note that the receiver temperature of VERA includes the temperature increase due to the feedome loss and the spill-over effect. In Mizusawa, typical system temperature in the K-band is  $T_{\rm sys}=150~{\rm K}$  in fine weather of winter season, but sometimes rises above  $T_{\rm sys}=300~{\rm K}$  in summer season. The system temperature at Iriki station shows a similar tendency to that in Mizusawa. In Ogasawara and Ishigakijima, typical system temperature is similar to that for summer in Mizusawa site, with typical optical depth of  $\tau_0=0.2\sim0.3$ . The typical system temperature in the Q-band in Mizusawa is  $T_{\rm sys}=250~{\rm K}$  in fine weather of winter season, and  $T_{\rm sys}=300-400~{\rm K}$  in summer season. The typical system temperature in Ogasawara and Ishigakijima in the Q-band is larger than that in Mizusawa also.

On the other hand, system noise temperature in C-band is stable around 100–150 K at all the VERA stations through all the season with typical zenith optical depth of  $\tau_0 = 0.03 \sim 0.04$ , although it sometimes show larger values due to extremely bad weather condition.

The typical system temperature in the K-band at all KVN stations is around 100 K in winter season. In summer season, it increases up to  $\sim 300$  K. In the Q-band, the typical system temperature is around 150 K in winter season and 250 K in summer season at Yonsei and Tamna. The system temperature of Ulsan in the Q-band is about

40 K lower than the other two KVN stations. This is mainly due to the difference in receiver noise temperature (see Table 5).

### 3.11 Calibrator Information

The NRAO VLBA calibrator survey is very useful to search for a continuum source which can be used as a reference source to carry out the delay, bandpass, and phase calibrations. The source list of this calibrator survey can be found at the following VLBA homepage,

http://www.vlba.nrao.edu/astro/calib/index.shtml.

For delay calibrations and bandpass calibrations, calibrators with 1 Jy or brighter are strongly recommended as listed in the VLBA fringe finder survey:

http://www.vlba.nrao.edu/astro/fringe\\_finder\\_survey/ffs.html. Interval of observing calibrator scans must be shorter than 1 hour to track the delay and delay rate in the correlation process.

If you request the participation of the YAM32 and/or KMRT40 antennas for observations in C-band, it is mandatory to do gain calibration and absolute flux scaling by the template spectrum method. In this method, a strong and compact CH<sub>3</sub>OH maser source which locates within 15° from the target source should be observed with an interval of 1 hr or shorter. In particular during elevations lower than 20°, it is recommended to observe these calibrators every 30 min or shorter. Even if YAM32 and/or KMRT40 antennas are not included in the observations, it is recommended to observe the strong and compact CH<sub>3</sub>OH maser source with the same interval as the cross-check for the gain curve and absolute flux scaling of the TMRT65 antenna as well. The 6.7 GHz CH<sub>3</sub>OH maser sources close to your target sources can be found in the following catalog papers (NOTE: in the template spectrum method for the TMRT65 in C-band, it is NOT recommended that the 6.7 GHz CH<sub>3</sub>OH maser sources 009.621+0.196, 133.94+1.04 (W3(OH) / W3-IRS5), and 351.417+0.645 & 351.417+0.646 (NGC6334F) are selected because these sources are too strong for the TMRT65 to guarantee an accuracy of the absolute flux scaling.):

## Methanol MultiBeam (MMB) Survey:

```
20^{\circ} \leq l \leq 60^{\circ}: \ \text{https://academic.oup.com/mnras/article/450/4/4109/1747594} \\ 6^{\circ} \leq l \leq 20^{\circ}: \ \text{https://academic.oup.com/mnras/article/409/3/913/1094145} \\ 345^{\circ} \leq l \leq 6^{\circ}: \ \text{https://academic.oup.com/mnras/article/404/2/1029/968927} \\ 330^{\circ} \leq l \leq 345^{\circ}: \ \text{https://academic.oup.com/mnras/article/417/3/1964/1090874} \\ 186^{\circ} \leq l \leq 330^{\circ}: \ \text{https://academic.oup.com/mnras/article/420/4/3108/972699} \\ \label{eq:definition}
```

#### Other catalog for sources in more northern hemisphere:

https://www.aanda.org/articles/aa/abs/2009/44/aa12135-09/aa12135-09.html

### 3.12 Data Archive

The users who proposed the observations will have an exclusive access the data for 18 months after the correlation. After that period, all data for EAVN open-use observations will be released as archive data. Thereafter, archived data will be available to any user upon request. This policy is applied to each observation, even if the proposed observation is comprised of multi-epoch observations in this season.

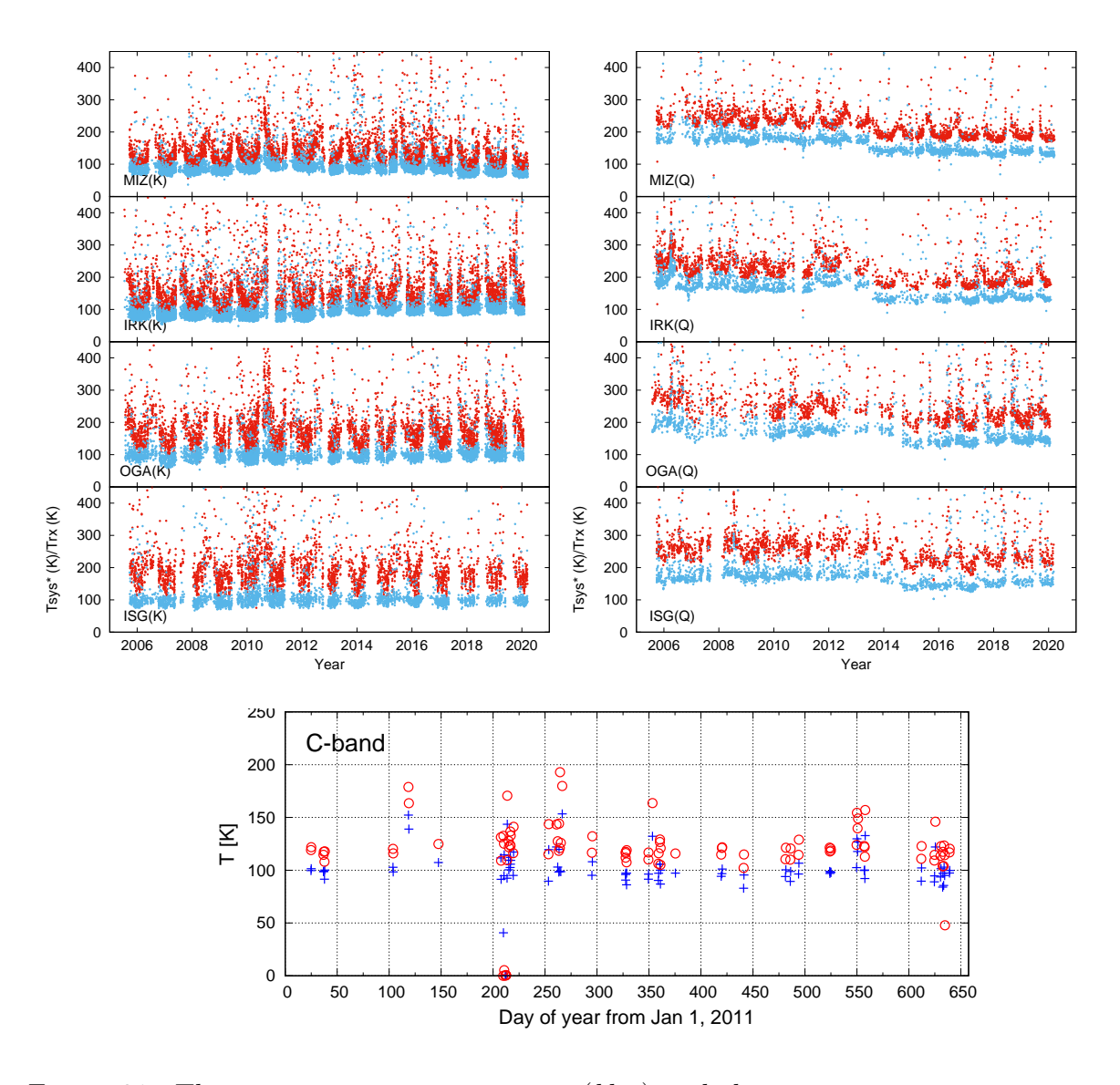


Figure 21: The receiver noise temperature (blue) and the system noise temperature (red) at the zenith for the VERA antennas at K-band (top-left), Q-band (top-right), and at C-band in Ogasawara station (bottom).

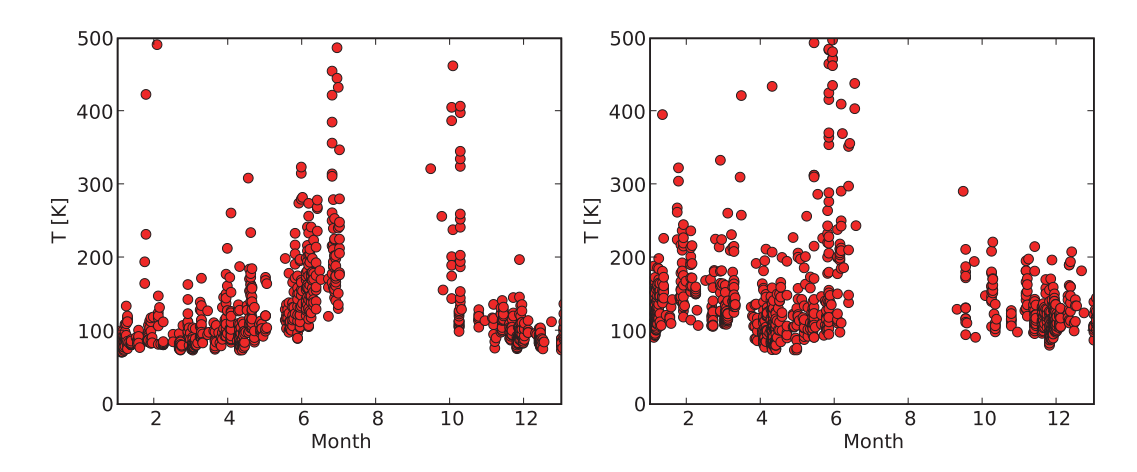


Figure 22: The zenith system noise temperature (red filled circles) at K-band (left) and Q-band (right) in KVN-Ulsan station.

Table 16: Image sensitivity of EAVN.

Array	$N_{ m ant}$	$N_{ m bl}$	C-band	K-band	Q-band
KVN	3	3	_	320	480
VERA	4	6	_	360	750
KaVA	7	21	_	219	379
KaVA+TMRT65	8	28	_	85	125
KaVA+NRO45	8	28	_	126	239
KaVA+TMRT65+NRO45	9	36	_	60	95
KaVA+TMRT65+NSRT26	9	36	_	63	_
KaVA+TMRT65+KSJ	9	36	_	76	113
KaVA+NRO45+KSJ	9	36	_	111	209
KaVA+TMRT65+NSRT26+NRO45	10	45	_	49	_
KaVA+TMRT65+NRO45+KSJ	10	45	_	56	89
KaVA+TMRT65+NSRT26+KSJ	10	45	_	59	_
KaVA+TMRT65+NSRT26+NRO45+TAK32	11	55	_	41	_
KaVA+TMRT65+NSRT26+NRO45+KSJ	11	55	_	46	_
KaVA+TMRT65+NSRT26+NRO45+TAK32+KSJ	12	66	_	39	_
KaVA+TMRT65	6	15	94	_	
KaVA+SHRT25	6	15	346	_	_
KaVA+KMRT40	6	15	203	_	_
KaVA+HIT32+YAM32	7	21	89	_	_
KaVA+TMRT65+KMRT40	7	21	58	_	_
KaVA+SHRT25+KMRT40	7	21	174	_	_
KaVA+TMRT65+HIT32+YAM32	8	28	37	_	_
KaVA+SHRT25+HIT32+YAM32	8	28	83	_	_
KaVA+HIT32+YAM32+KMRT40	8	28	65	_	_
KaVA+TMRT65+HIT32+YAM32+KMRT40	9	36	31	_	_
KaVA+SHRT25+HIT32+YAM32+KMRT40	9	36	62		

Note:  $N_{\rm ant}$  and  $N_{\rm bl}$  are the numbers of telescopes and baselines for each array, respectively. The  $1\sigma$  image sensitivity values are listed in unit of  $\mu \rm Jy$ , which assume an integration time of 4 hours and a total bandwidth of 256 MHz for the calculation. In the case of narrower bandwidth of 15.625 kHz (for maser emission in K/Q-bands) and 1.953 kHz (for maser emission in C-band), sensitivities can be calculated by multiplying a factor of 128 and 362, respectively.

# 4 Notes for Special Modes

In this section, we summarize additional information about special observing/data analysis modes.

## 4.1 Phase-referencing and Astrometry

EAVN is capable of phase-referencing observations to image weak target sources, which cannot be detected within coherent time, and to conduct absolute astrometry measurements. Note that astrometry capability has been confirmed for K-band observations with KaVA 7 telescopes. Although we do not prevent EAVN proposers from submitting proposals with the phase-referencing mode at Q-band and/or with the mode using non-KaVA telescopes within the maximum driving speed of each antenna shown in Table 3, the data quality is not guaranteed. From the semester 2021A, we opened the fast-switching (not astrometry mode) mode in C-band as well. In 2022A, the following antenna combination among KaVA+HIT32+YAM32+SHRT25+KMRT40 is available (see the notification in sub-section 4.1.1).

### 4.1.1 Fast Switching

Fast switching observation with EAVN is recommended for phase referencing (and astrometry) since the verification of the fast switching with EAVN has been finished, except for TMRT65, NRO45 and TAK32 telescopes. In this mode, the antenna nods between phase calibrator (reference) and target source. With this mode, we can detect and image weak sources, which can not be imaged directly by fringe fitting. Regarding antenna switching cycle, users can refer to Table 17.

## 4.1.2 Notification for Switching Cycle in C-band

In the fast-switching in C-band, we recommend typical time of each switching cycle of 5–6 min, which was observationally verified successful phase-referencing imaging without serious issues and a few milliarcsecond accuracies of absolute position measurements. When you decide the switching cycle, it is necessary to take into account the slewing time of HIT32 that has the slowest driving speed of  $0.2^{\circ}$  sec<sup>-1</sup>. We thus present a simulated result of antenna slewing time of HIT32. Figure 23 plots the relationship between the slewing time in one way between target and reference continuum sources as a function of elevation angles for the target–calibrator separation angles (S.A.) of 1 and 2 deg. From Figure 23, it is strongly recommended to schedule the fast-switching observations with elevation angles lower than 80 and 70 deg in the case of S.A. of 1 and 2 deg, respectively. Finally, proposers are required to specify each on-source time for target and reference continuum sources in one switching cycle at C-band in scientific or technical justification in the proposal.

#### 4.1.3 Separation Angle between Target and Phase Reference

It is strongly recommended to observe a pair sources with a small separation angle (e.g., less than 1 degree) at high elevation for precise astrometry. For instance, it

Table 17:	Phase-R	eferencing	Cycle	Times (	min	).*
			/			/

				J •			
	Typic	cal weather	Bad	weather	Good	weather	
	$(C_n^{\dagger} = 1)$	$2 \times 10^7 \text{ m}^{-1/3}$	$(C_n^{\dagger} = 4)$	$4 \times 10^7 \text{ m}^{-1/3}$	$(C_n^{\dagger} = 1 \times 10^7 \text{ m}^{-1/3})$		
	Frequ	ency (GHz)	Freque	Frequency (GHz)		acy (GHz)	
EL (deg)	$22   (43)^{\ddagger}$		22	$(43)^{\ddagger}$	22	$(43)^{\ddagger}$	
5	0.3	0.2	0.2	0.1	0.8	0.4	
10	0.5	0.3	0.2	0.1	0.8	0.6	
15	0.7	0.3	0.3	0.1	1.5	0.7	
20	0.8	0.4	0.3	0.2	1.8	0.9	
25	0.9	0.4	0.4	0.2	2.0	1.0	
30	1.0	0.5	0.4	0.2	2.8	1.1	
40	1.1	0.5	0.5	0.2	5.8	1.3	
50	1.3	0.6	0.6	0.3	9.9	1.5	
60	1.8	0.7	0.6	0.3	10.0	2.2	
70	2.3	0.7	0.6	0.3	10.0	2.9	
80	2.6	0.7	0.6	0.3	10.0	3.3	

<sup>\*</sup> Referring to Ulvestad, J., Phase-Referencing Cycle Times, VLBA Scientific Memo 20 (1999).

Column 1 shows antenna elevation angles. Columns 2-3 indicate phase-referencing cycles at 22 and 43 GHz, respectively, under typical weather condition. The phase-referencing cycle is defined as the time between the midpoints of the two calibrator observations before and after the target observation. Columns 4-5 are the same as Columns 2-3, but with bad weather condition (similar to some summer days). Columns 6-7 are the same as Columns 2-3, but with good weather condition (similar to some winter nights).

is demonstrated that the dynamic range of the phase-referenced image is inversely proportional to the sine of the calibrator-to-target separation as

$$D_1 = \left(\frac{\sqrt{\Delta t}}{K\nu}\right) \left(\sin\theta_{\text{sep}}\right)^{-1},\tag{6}$$

where  $\Delta t$  is the on-source observing time,  $\nu$ , the observing frequency,  $\theta_{\text{sep}}$ , the separation angle between the target and calibrator, and K, a constant to be determined [13].

## 4.1.4 Tropospheric Calibration with GPS or JMA or Geodetic Blocks

Generally, residual of atmospheric zenith delay dominates cm-wave VLBI positional accuracy. Atmospheric (tropospheric) calibration for EAVN has three options (see Table 18), which are (1) GPS, (2) Japan Meteorological Agency (JMA) meso-scale analysis data (Hobiger et al. 2008; JMA Numerical Weather Prediction<sup>1</sup>), and (3) Geodetic blocks<sup>2</sup>. An error of tropospheric zenith delay ( $c\Delta\tau_{trop}$ ) can be suppressed within  $\sim$ 2 cm with GPS, JMA and Geodetic blocks [9, 14].

#### 4.1.5 Astrometric Accuracy

We have verified astrometric accuracy with KaVA and EAVN, based on (1) a Galactic line source and (2) QSO pair observations (see Figures 24 and 25, and Tables 19 and

<sup>&</sup>lt;sup> $\dagger$ </sup>  $C_n$  is strength of the tropospheric turbulence.

<sup>&</sup>lt;sup>‡</sup> Currently, Q-band phase-referencing mode is under evaluation.

<sup>&</sup>lt;sup>1</sup>https://www.jma.go.jp/jma/jma-eng/jma-center/nwp/nwp-top.htm

<sup>&</sup>lt;sup>2</sup>http://bessel.vlbi-astrometry.org/tech

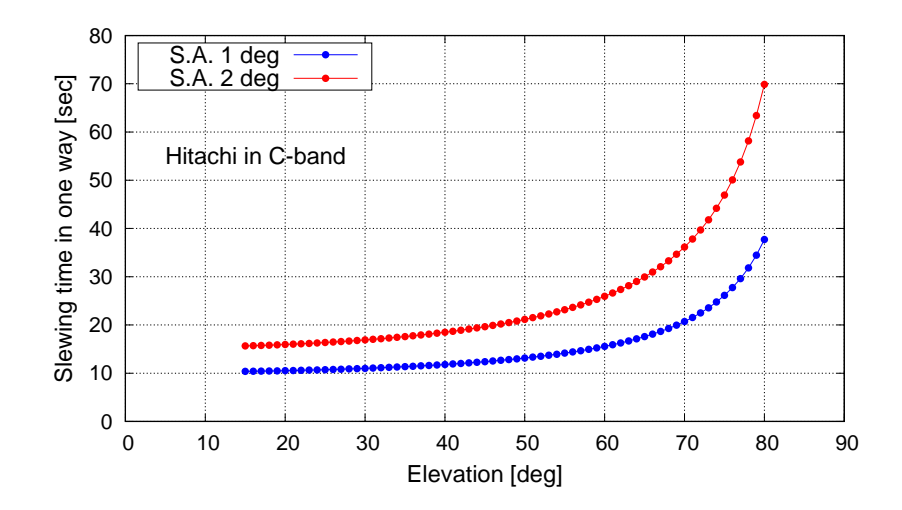


Figure 23: Simulated result of antenna slewing time of HIT32 at C-band in one way between target and reference continuum sources. This simulation shows a dependence on elevation, and a difference in the case of the separation angle of 1 deg (blue filled circles) and 2 deg (red filled circles).

Table 18: Tropospheric calibration for each EAVN telescope\*.

Telescope		Method									
	GPS	GPS JMA Geodetic blocks									
KaVA	•	•	•								
TMRT65	$\triangle$	•	•								
NSRT26	$\triangle$	×	•								

<sup>\*</sup> TMRT65 = Tianma 65m. NSRT26 = Nanshan 26m.  $\bullet$  = Available.  $\triangle$  = It would be available in the near future.  $\times$  = Not available.

20). Single-epoch (relative) astrometric error consists of (1) thermal and (2) systematic errors as shown below [18]:

$$\Delta\theta_{\text{therm}} \approx 12 \left(\frac{\lambda[\text{cm}]}{1.3}\right) \left(\frac{B[\text{km}]}{2,300}\right)^{-1} \left(\frac{\text{S/N}}{20}\right)^{-1} [\mu \text{as}],$$
 (7)

and

$$\Delta s_{\rm rel} \approx 31 \left(\frac{{\rm c}\Delta \tau [{\rm cm}]}{2}\right) \left(\frac{B[{\rm km}]}{2,300}\right)^{-1} \left(\frac{\theta_{\rm sep}[{\rm deg}]}{1}\right) [\mu {\rm as}],$$
 (8)

where  $\lambda$  is the observing wavelength, B, the longest baseline length, S/N, signal-to-noise ratio of (phase-referenced) image,  $c\Delta\tau$ , the speed of light multiplied by delay residual, and  $\theta_{\rm sep}$ , separation angle between target and calibrator (phase reference).

#### 4.1.6 Baseline Length

The longest baseline length is related to astrometric accuracy as shown in Equations (7) and (8). Baseline lengths for EAVN astrometry are compiled in Table 21.

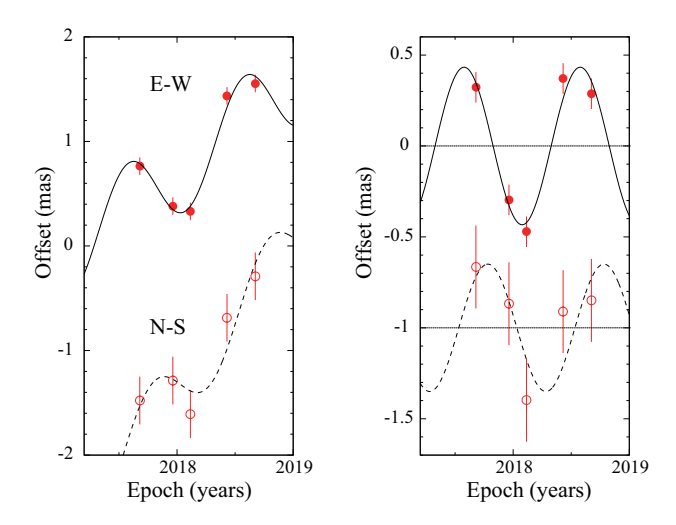


Figure 24: Results of parallax and proper-motion fitting. Plotted are position offset of maser spot (W3(OH) at  $V_{\rm LSR} = -47.5~{\rm km~s^{-1}}$ ) with respect to the background QSO J0244+6228 (with a separation angle of 2.2 degrees) toward the east (R.A.cos $\sigma$ ) and north ( $\sigma$ ) as a function of time. For clarity, the north direction data is plotted offset from the east direction data. (*Left*) The best-fit models in the east and north directions are shown as continuous and dashed curves, respectively. (*Right*) Same as the Left, but with proper motions removed.

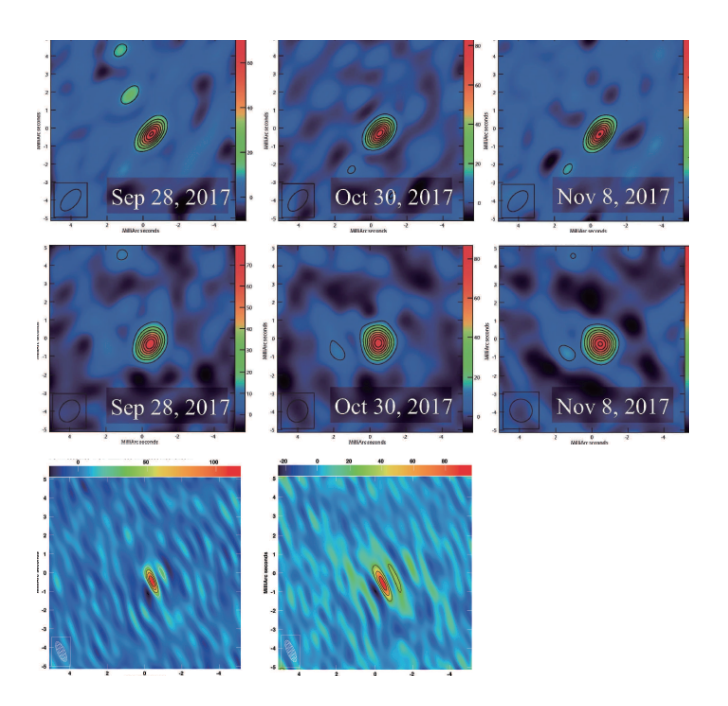


Figure 25: (**Top row**) Phase-referenced images of 0556+238 with VERA, relative to the phase reference 0601+245. The dates of the observations are Sep 28, Oct 30 and Nov 8 in 2017 from left to right. (**Middle row**) Same as the top row, but for KaVA data used. (**Bottom row**) Same as the top row, but for EAVN data used. Observation dates are Mar 27 and May 24 in 2019 from left to right.

Table 19: Parallax results for  $W3(OH)^*$ .

Array	Frequency	Source	$V_{ m LSR}$	Parallax	$\sigma_{lpha { m cos} \delta}^*$	${\sigma_\delta}^*$	Ref.
	GHz		${\rm km~s^{-1}}$	(mas)	(mas)	(mas)	
KaVA	22	W3OH	-47.5	$0.460 {\pm} 0.035$	0.052	0.256	
VLBA	22	W3OH	$-51.5 \sim -48.2$	$0.489 \pm 0.017$	$\sim 0.050$	$\sim \! 0.050$	(1)

<sup>\*</sup>Positional errors in right ascension and declination were adjusted so that the reduced chi-square becomes unity. Columns 1-2 represent array and observing frequency. Columns 3-4 show source name and LSR velocity of the maser spot, used for the parallax fit. Column 5 displays the parallax result in milli-arcseconds (mas). Columns 6-7 represent the (systematic) positional errors in right ascension and declination, respectively.

Ref. (1) Hachisuka et al. (2006).

Table 20: Results of position repeatability for 0556+238.

100	Table 20. Results of position repeatedsinty for 6500 (200.										
	VE	ERA	Ka	VA	EA	VN					
Observation date	R.A.	Decl.	R.A.	Decl.	R.A.	Decl.					
	$(\mu as)$	$(\mu as)$	$(\mu as)$	$(\mu as)$	$(\mu as)$	$(\mu as)$					
2017/Sep/28	$-465 \pm 15$	$-332 \pm 16$	$-451 \pm 15$	$-331 \pm 15$	_	_					
$2017\mathrm{Oct}/30$	$-494 \pm 11$	$-283 \pm 12$	$-462 \pm 16$	$-258 \pm 18$	_	_					
2017/Nov/8	$-505 \pm 09$	$-318 \pm 10$	$-480 \pm 13$	$-287 \pm 14$	_	_					
$2019/\mathrm{Mar}/27$	$-463 \pm 21$	$-343 \pm 24$	$-464 \pm 14$	$-336 \pm 17$	$-407 \pm 11$	$-455 \pm 21$					
2019/May/24	$-576 \pm 85$	$-479 \pm 150$	$-592 \pm 29$	$-434 \pm 35$	$-411 \pm 24$	$-524 \pm 44$					
Unweighted mean	$-500\pm21$	$-351 \pm 34$	$-490 \pm 26$	$-330 \pm 30$	$-409 \pm 2$	$-490 \pm 35$					

Column 1 shows the date of observation. Columns 2-3 display image positions of 0556+238 relative to 0601+245 in right ascension and declination, respectively. Note that the image positions were measured for VERA data. The errors of the positions represent the thermal error. Columns 4-5 are the same as the Columns 2-3, but for KaVA data used. Columns 6-7 are the same as the Columns 2-3, but for EAVN data used.

### 4.1.7 A priori Model of the KJCC Correlator

The initial delay tracking model at the KJCC correlator is not sufficient for high precision position measurement. Therefore, we provide a calibration table (called as the delay re-calculation table) to PIs, where the necessary information such as the latest station coordinates, the most-updated Earth-rotation parameters, tropospheric and ionospheric delays is included. The table can be loaded with the AIPS task "TBIN".

In order to prepare these calibration information, the delivery of data and calibration tables will take about three months after the observation.

#### 4.1.8 Data Reduction

Generally, users are encouraged to carry out data reduction in consultation with contact person and/or support scientist in the KaVA/EAVN project group. Procedure of astrometric data reduction for VERA data has been summarized in previous papers (e.g. Fig. 11 in [11]; Fig. 5 in [10]). Basically, the procedure of data reduction for KaVA/EAVN data is consistent with that for VERA data, expect for few points.

For instance, parallactic angle should be corrected if the fast switching observation is conducted with single beam. The NRAO AIPS task "CLCOR" can be used for the calibration by setting the OPCODE = "PANG".

Table 21: Baseline lengths for EAVN astrometry.\*

	MIZ	IKK	OGA	ISG	KYS	KUS	KIN	$1\mathrm{M}65$	NS26	SH25	H1132	YAM32	KM40
MIZ													
IRK	1,300												
OGA	1,300	1,300											
ISG	2,300	1,000	1,800										
KYS	1,200	700	1,800	1,500									
KUS	1,100	400	1,500	1,300	300								
KTN	1,500	400	1,700	1,000	500	400							
TM65	2,000	900	2,100	800	900	900	600						
NS26	4,500	4,000	5,200	4,000	3,400	3,700	3,600	3,300					
SH25	2,000	900	2,100	800	_	900	_	_	_				
HIT32	300	1,100	1,100	2,100	_	1,000	_	1,900	_	1,900			
YAM32	1,000	300	1,300	1,300	_	300	_	1,000	_	1,000	900		
KM40	3,900	2,800	3,900	2,200	_	2,800	_	1,900	_	1,900	3,800	2,900	
KSJ	1,300	600	1,800	1,400	100	200	400	800	3,400	_	_	_	_

<sup>\*</sup> The unit is (km). Each value is rounded off to the (nearest) 100. MIZ=VERA-Mizusawa; IRK=VERA-Iriki; OGA=VERA-Ogasawara; ISG=VERA-Ishigakijima; KYS=KVN-Yonsei; KUS=KVN-Ulsan; KTN=KVN-Tamna; TM65=TMRT65; NS26=NSRT26; SH25=SHRT25; KM40=KMRT40; KSJ=Sejong22.

# 4.2 1-beam Hybrid (K/Q/W) Mode

1/17

KaVA will enable us to conduct VLBI observations in combinations of different types of antennas (antenna beams), receiving bands, recording rates (namely total band widths), and filtered base band channels in one observing session, whose cross correlation is still valid for the whole or some parts of KaVA. In such "hybrid" observing modes with KaVA, there are some modes that are available in the 2022A CfP described as follows.

Although VERA shall use only one of dual beams in a single frequency band (K or Q), the KVN is able to observe in two to three of K/Q/W bands simultaneously in a common observing session. Please check the KVN status report for W-band information (https://radio.kasi.re.kr/status\\_report/status\\_report.php?site=kvn). Signal correlation for all the KaVA baselines is valid for the band in which both the KVN and VERA observe, while that for all the observed bands is valid for the KVN baselines.

Frequency allocations should be made separately to the KVN and VERA, including base band channels that are common between the two arrays in a specific band (K or Q). Note that the number of base band channels or the total bandwidth available per frequency band is limited, therefore brighter continuum sources should be selected for group-delay calibration.

# 4.3 Wide-field Imaging Mode

This mode is required to fully image 44 GHz methanol maser emissions associated with star-forming regions, which are generally distributed on the angular scale over 10 arcsec. The wide-field imaging (WFI) mode is achieved with an accumulation period shorter than the usual one of 1.6384 sec in Daejeon correlator at KJCC. Theoretically, the field

of view (FoV) within an amplitude loss of 1%, 5%, and 10% is estimated on the basis of the time-average smearing effect due to a finite accumulation period [22]. The FoVs calculated for accumulation periods of 0.2048, 1.6384, and 3.2768 sec are summarized in Table 22, in the case of the highest angular resolution at Q-band of 0.6 mas with KaVA.

Table 22: FoV within a given amplitude loss in each accumulation period\*.

	Aı	mplitude lo	OSS
	1.0%	5.0%	10.0%
Accumulation period	FoV	FoV	FoV
(sec)	(arcsec)	(arcsec)	(arcsec)
0.2048	8.6	19.4	27.4
1.6384	1.1	2.4	3.4
3.2768	0.5	1.2	1.7

<sup>\*</sup> Under an assumption of the highest angular resolution at Q-band of 0.6 mas with KaVA.

In the current available specification of Daejeon correlator, there is a trade-off between a shorter accumulation period and a larger number of IF channels to yield higher spectral resolution. The most highly recommended setup is the combination of C2 mode and an accumulation period of 0.2048 sec, in which both a sufficiently high velocity resolution (0.11 km s<sup>-1</sup> for 44 GHz methanol masers) and a sufficiently wide FoV (10 arcsec or more) can be obtained. Thus the recommended set-up for WFI mode is summarized in Table 23.

Table 23: Recommended set-up for WFI mode in the current situation.

Correlation	Sampling	Bandwidth	Accumulation	Spectral
mode	rate	$/\mathrm{IF}$	period	channels/IF
C2	1024 Mbps	128 MHz	$0.2048  \sec$	8,192

The evaluation for the WFI tests was done by the following two ways: comparing the data of an accumulation period of 0.1 sec produced in DiFX to those of 0.2048 sec in Daejeon correlator, and comparing the latter data to the same data but with averaging in 3.2768 sec. These ways provide us a chance to estimate whether such an isolated maser can be detected or not and how much rate of the amplitude loss occurs. The evaluation might be updated on the basis of a comparison between a short-accumulation period data and a multi-tracking center data in the near future.

If you would like to require this WFI mode, please describe your requests in the following two items:

- Requested setting parameters for WFI in the proposal cover sheet
- Reasons for requiring WFI mode in the scientific justification

Finally, note that the file size of correlated data for WFI is as huge as ~600 GByte. We therefore recommend to check and improve the performance of your internet environment and personal computer as high as possible for comfortable data downloading and data processing, respectively. Please refer an example parameters in Table 24:

Table 24: Required performances of internet and personal computer.

Forward speed	$\geq 10 \text{ MByte s}^{-1}$
HDD/SSD volume	$\geq 1.5 \text{ TByte}$
RAM	$\geq 16$ GByte

Here, the experiment to verify the time-average smearing effect due to a finite accumulation period has been done, however we will also verify the bandwidth smearing effect to KaVA observations in the near future.

## 4.4 Simultaneous K/Q Band Mode

Simultaneous K/Q-band data reception mode is available for KaVA, NRO45, and KSJ on a limited basis for open-use. Please note the following limitation: (1) K/Q simultaneous observations cannot be performed regularly but will be performed by setting up to two sessions in 2022A semester (where each slot spans approximately one—two week(s)) because VERA requires a special setup at the front-end for K/Q simultaneous reception. (2) The frequency setup is fixed as shown in Table 25. The term of K/Q session will be determined depending on requests of approved proposals. (3) Frequency phase transfer (FPT) technique [21] is not applicable to the data obtained at NRO45. (4) 'Template method' for the amplitude calibration should be employed to the data obtained at NRO45 since the system noise temperature cannot be measured using the K/Q-band simultaneous reception system at Nobeyama.

Table 25: Frequency setup for simultaneous K/Q band observation

	1 0 1	/ •	
Band	Frequency range	BBC channel	Polarization
K-band	22.112 - 22.240 MHz	32 MHz x 4 channels	RHCP
Q-band	42.812 - 42.940 MHz	$32~\mathrm{MHz}$ x 4 channels	LHCP

A demonstrative observation and detailed performance of simultaneous K/Q-band observations with KaVA is presented in the Zhao et al. (2019). You can also check science cases with simultaneous multi-frequency VLBI observations [5].

# 5 Observation and Data Reduction

## 5.1 Preparation of an EAVN Observation

After the acceptance of proposals, users are requested to prepare the observing schedule file two weeks before the observation date. The observer is encouraged to consult a contact person in the EAVN Array Operation Center (AOC) and/or the User Support Team (UST) to prepare the schedule file. The schedule submission should be done by a stand-alone vex file. The examples of EAVN vex file are available at the EAVN web site:

http://radio.kasi.re.kr/kava/kava\_observing\_preparation.php Detailed information about preparation and submission of a schedule file for TMRT65 and NRO45 will be announced when distributing the proposal review results.

On your schedule, we strongly recommend to include at least two fringe finder scans, each lasting 5 or more minutes at the first and latter part of observation in order to search the delay and rate offsets for the correlation.

For EAVN which includes the large telescopes (TMRT65 and NRO45), regular pointing check is necessary at both K- and Q-bands. You should leave a 8-15 min gap every  $\leq 1-2$  hr in your schedule file to allow this. Pointing check is done by the local operators. In addition, we strongly recommend to include frequent scans of a maser source and/or a bright compact continuum source located within 15° from the target. This allows a cross check of the amplitude calibration for TMRT65 and NRO45 along with the usual a priori method.

If you request the participation of the YAM32 and/or KMRT40 antennas at C-band, it is mandatory to do gain calibration and absolute flux scaling by the template spectrum method. In this method, a strong and compact CH<sub>3</sub>OH maser source that locates within 15° from the target source is observed with an interval of 1 hr or shorter. In particular during elevations lower than 20°, it is recommended to observe these calibrators every 30 min or shorter. Even if the YAM32 and/or KMRT40 antennas are not included, it is recommended to observe the strong and compact CH<sub>3</sub>OH maser source with the same interval as the cross-check for the gain curve and absolute flux scaling of the TMRT65 antenna as well. To select calibrators appropriated to your target sources, please see Section 3.11.

We request PIs to specify their correlation parameters at the beginning of the vex file for proper correlation processing. In particular, PIs who request for sub-array or dual-beam observations for EAVN should provide a frequency matching table for the correct correlation. In the case of any observations for CH<sub>3</sub>OH masers at 6.7 GHz in C-band, it is strongly recommended to request the C5 correlation mode (16 MHz  $\times$  16 IFs) and the maximum spectral channels 8,192 for IF5 including the maser emission (corresponding to RF 6,664–6,680 MHz with the normal frequency set-up) to achieve the sufficient channel resolution of 1.953 kHz, yielding to the velocity resolution of  $\sim$ 0.088 km s<sup>-1</sup>.

#### 5.1.1 Sample Key Files for NRAO sched

EAVN UST will provide sample key files to be used for preparation of schedule files. These are collection of the inputs for the NRAO sched software. Files are available on

the EAVN website:

https://radio.kasi.re.kr/eavn/notice\_user.php

For more details of NRAO sched, please refer to the NRAO website:

https://science.nrao.edu/facilities/vlba/docs/manuals/propvlba/sched

The above sample key files take into account special settings optimized to EAVN observations (e.g. fixed/nominal frequency setting recommended/required for each telescope). Thus, the EAVN users are strongly recommended to use the above sample key files. The detailed information will be updated on the EAVN website.

### 5.2 Observation and Correlation

EAVN members take full responsibility for observation and correlation process, and thus basically proposers will not be asked to take part in observations or correlations. Observations are proceeded by operators from each array and telescope, and correlated data is delivered to the users in approximately two months including the time for media shipping to KJCC at Daejeon.

After the correlation, the user will be notified where the data can be downloaded by e-mail. After one month later of a correlated data distribution to PIs, disk modules which contains raw observing data can be recycled without notice. Therefore, PIs should investigate the correlated output carefully. For re-correlation or raw data keeping of the data, PI should provide adequate evidence in order to justify his/her request. If there is an issue related to correlated data, PI should contact with the EAVN UST or the correlator team (kjcc (at-mark) kasi.re.kr), and not to ask KJCC members directly.

### 5.3 Data Reduction

For EAVN data reduction, the users are encouraged to reduce the data using the NRAO AIPS software package. The observation data and calibration data will be provided to the users in a format which AIPS can read.

As for the amplitude calibration, we will provide "ANTAB" files which include the system temperature information measured by the R-sky method and the information of the dependence of aperture efficiency on antenna elevation, except YAM32 and KMRT40 antennas where the gain calibration and absolute flux scaling have to be achieved via the template spectrum method in the AIPS task "ACFIT". A sample script for the template spectrum method is available on the EAVN website (see section 5.3.1). If the user needs weather information, the meteorological data of the temperature, pressure, and humidity during the observation can be provided.

In case of questions or problems, the users are encouraged to ask the contact person in EAVN members and/or the EAVN UST.

#### 5.3.1 Sample AIPS Recipes

EAVN UST will provide sample recipes for data calibration and imaging by using AIPS. These are simple script files for the following observation settings:

- KaVA observation of the 22 GHz H<sub>2</sub>O maser
- EAVN observation of the 6.7 GHz CH<sub>3</sub>OH maser
- EAVN phase-referencing observation at K-band
- RUN file for the KaVA phase-referencing astrometry of the 22 GHz H<sub>2</sub>O maser

A sample script for the amplitude calibration procedure via the template spectrum method is available. Files are available the following EAVN web site:

https://radio.kasi.re.kr/eavn/data\_reduction.php

While these files cover only widely used basic setting but not all the available observation modes, they can be modified for your observation mode.

## 5.4 Policy of User Support

From the 2021A semester, EAVN will not assign any support scientists to all the accepted proposals. If the proposers/observers have any inquiry about EAVN observations, they should contact with the EAVN UST and/or the relevant addresses as listed in Table 26. If the proposers need extensive support by the EAVN experts for schedule preparation and data analysis, they can request to assign a support scientist in the proposal cover sheet. UST will arrange the support scientist to the accepted proposals which request extensive support considering their science cases and its necessity.

# 5.5 Acknowledgment

All EAVN users (both proposers for using EAVN and data analysts using EAVN archive data) are asked to specify the following acknowledgment (or similar one) to EAVN in their publications.

This work is made use of the East Asian VLBI Network (EAVN), which is operated under cooperative agreement by National Astronomical Observatory of Japan (NAOJ), Korea Astronomy and Space Science Institute (KASI), Shanghai Astronomical Observatory (SHAO), Xinjiang Astronomical Observatory (XAO), Yunnan Astronomical Observatory (YNAO), and National Geographic Information Institute (NGII), with the operational support by Ibaraki University (for the operation of HIT32 and TAK32), Yamaguchi University (for the operation of YAM32), and Kagoshima University (for the operation of VERA Iriki antenna).

Please include participating telescopes of your project in Acknowledgment of your publications.

### 5.6 Further Information

The users can contact any staff member of EAVN by e-mail (see Table 26). Note that your EAVN proposal should be submitted to the following EAVN proposal submission site.

https://radio.kasi.re.kr/eavn/proposal info.php

Table 26: Contact addresses.

Name	E-mail address	Related Field
Inquiry about	eavnprop (at-mark) kasi.re.kr	Proposal-related requests/questions
proposal submission		
User support team	eavnhelp (at-mark) kasi.re.kr	User support in general
Operation team	eavnobs (at-mark) kasi.re.kr	Observation-related requests/questions,
		schedule submission
Correlator team	kjcc (at-mark) kasi.re.kr	Correlation-related requests/questions,
		correlated data distribution

# References

- [1] EAVN Status Report for the 2021B Semester: https://radio.kasi.re.kr/kava/status\_report21b/node3.html
- [2] NRO web site: http://www.nro.nao.ac.jp/~nro45mrt/html/index-e.html
- [3] Cho, I. et al. 2017, PASJ, 69, 87
- [4] Cui, Y. Z. et al. 2021, RAA, in press (http://arxiv.org/abs/2104.05525)
- [5] Dodson, R. et al. 2017, ApJ, 834, 177
- [6] Hachisuka, K. et al. 2006, ApJ, 645, 337
- [7] Han, S.-T. et al. 2008, Int. J. Infrared Millimeter Waves, 29, 69
- [8] Han, S.-T. et al. 2013, PASP, 125, 539
- [9] Honma, M. et al. 2008, PASJ, 60, 951
- [10] Imai, H. et al. 2012, PASJ, 64, 142
- [11] Kurayama, T. et al. 2011, PASJ, 63, 513
- [12] Lee, S.-S. et al. 2015, JKAS, 48, 229
- [13] Martí-Vidal, I. et al. 2010, A&A, 515, 53
- [14] Nagayama, T. et al. 2015, PASJ, 67, 65
- [15] Oh, S.-J. et al. 2011, PASJ, 63, 1229
- [16] Ott, M. et al. 1994, A&A, 284, 331
- [17] Oyama, T. et al. 2016, PASJ, 68, 105
- [18] Reid, M. J. & Honma, M. 2014, ARA&A, 52, 339
- [19] Yonekura, Y. et al. 2016, PASJ, 68, 74
- [20] Yoo, S. M. et al. 2018, JKAS, 51, 143
- [21] Zhao, G. Y., et al. 2019, JKAS, 52, 23

[22] Proceedings from the 1988 synthesis imaging workshop in NRAO, Chapter 13 in Synthesis Imaging in Radio Astronomy: A Collection of Lectures from the Third NRAO Synthesis Imaging Summer School (http://www.aspbooks.org/a/volumes/table\_of\_contents/?book\_id=118)